TN-1156

Technical Note N-1156

WAVE ENERGY EXTRACTION BY CRESCENT SHAPED COLUMNS FOR STATION KEEPING OF FLOATING OCEAN PLATFORMS - HYDRAULIC MODEL AND FEASIBILITY STUDY

By

C. L. Liu, Ph.D. and R. H. Fashbaugh, Ph.D.

March 1971

Approved for public release; distribution unlimited.

NAVAL CIVIL ENGINEERING LABORATORY
Port Hueneme, California 93041

TA
417
.N3
no.N1156

WAVE ENERGY EXTRACTION BY CRESCENT SHAPED COLUMNS FOR STATION KEEPING OF FLOATING OCEAN PLATFORMS - HYDRAULIC MODEL AND FEASIBILITY STUDY

Technical Note N-1156

ZF 38.512.001.017
03-001

by

C. L. Liu, Ph.D. and R. H. Fashbaugh, Ph.D.

ABSTRACT

Fixed or floating column-supported platforms in the ocean experience direct and reverse wave drag caused by the oscillating water particle velocity. The drag coefficient for the direct flow can be different from that for the reverse flow if the cross-sectional area of the supporting column is not symmetric about the column axis. Therefore, a net wave drag force theoretically can be produced. The purpose of this study was to determine whether this concept can be utilized to reduce the power requirements for positioning large floating platforms such as the proposed Mobile Ocean Basing System (MOBS).

Two support column cross sections were chosen for evaluation; a semi-circle and a crescent shape which is formed by two intersecting circles (the larger circle having a radius 1-1/2 times that of the smaller circle). A circular cross section was included to provide a reference. Free drift velocity tests of three small scale tri-column platforms with the three different cross sections were made in a small wave tank as a preliminary experiment. Based on the results of this drift experiment wave drag measurements were made with larger single column models of 4 inch diameter and 8 foot length in a large wave tank. Free drift velocity tests were also conducted with a 14 inch by 17 inch rectangular model floating platform with 36 supporting columns to aid in evaluating the concept for MOBS use.

The results of the tests show that there is a net wave force opposite to the direction of wave travel on the column with the crescent cross section. However, an analytical study based on the test data shows the rate of energy extraction from waves by crescent shaped columns for sea state 5 to be about 6% of the energy required for station keeping of a large floating platform. Hence, the concept does not seem applicable to large floating ocean platforms.

Approved for public release; distribution unlimited.

CONTENTS

PART I. HYDRAULIC SCALE MODEL STUDY

	page
INTRODUCTION	1
BACKGROUND	1
PRELIMINARY TESTS - DRIFT OBSERVATIONS	4
PRINCIPAL TESTS - WAVE FORCE MEASUREMENTS	11
RESULTS	16
FINDINGS	17
CONCLUSIONS OF HYDRAULIC MODEL STUDIES	18
REFERENCES	39
NOMENCLATURE	40

PART II. THE FEASIBILITY OF HYDRODYNAMIC FORMS FOR STATION KEEPING OF A LARGE FLOATING PLATFORM

	page
INTRODUCTION	43
ESTIMATION OF HYDRODYNAMIC FORM EFFECTIVENESS	44
MODEL TEST	48
CONCLUSIONS	50
APPENDIX A	55
APPENDIX B	56
REFERENCES	58

FORWORD

This Technical Note is concerned with the extraction of energy from ocean waves by vertical columns which have a cross section of crescent shape (which have been termed hydrodynamic forms in this report). It consists of two parts: Part I in which is reported the results of a hydraulic scale model test and Part II in which the practicability of using such columns for partial station keeping of large floating ocean platforms is investigated.

PART I. HYDRAULIC SCALE MODEL STUDY

by

C. L. Liu, Ph.D.

INTRODUCTION

There has been an increasing need for locating tactical and strategic bases in various parts of the world. A potential solution to this problem is huge ocean-borne platforms which could provide the area for such bases. One concept for a large platform is the Mobile Ocean Basing System (MOBS) which consists of floating platform modules connected together. This concept is similar to the concept of the FLoating AIRport (FLAIR) recently developed by Mr. Paul Weidlinger.[1] MOBS, however will be positioned in much deeper water and farther from shore than FLAIR.

One of the necessary requirements for MOBS is the capability to maintain position within a selected region of the ocean. Conventional spread moorings, deep taut line moorings, and dynamic positioning are examples of methods for controlling surface position of platforms. The large size of the proposed ocean-based structures requires large mooring lines, huge anchors and/or large propulsion power. All of these are difficult to realize. However, if the wave drag can be reduced or even utilized to provide resistance to wind and current drag, the mooring requirements will be reduced, hopefully, eliminating the need for special mooring gears and expensive propulsion power.

This report presents and evaluates a hypothesis which states that wave energy can be extracted by properly orienting vertical non-symmetric cylinders in regular waves. Net wave forces along and against the direction of wave propagation may be produced due to the difference in drag coefficients at the front and the rear of a non-symmetric cylinder. The report contains the results of a free drift experiment and a wave force model study for the verification of the hypothesis.

BACKGROUND

Hydrodynamic drag force on an object is generally expressed in terms of fluid kinetic pressure, cross-sectional area normal to the flow, and a drag coefficient. The drag formula can be written as[2]

$$F = C_D \cdot A \cdot \frac{\rho U^2}{2} \qquad (1)$$

where, F = total drag force on object, lb
C_D = drag coefficient
A = cross-sectional area of object, ft^2
ρ = fluid mass density, $slug/ft^3$
U = flow velocity, ft/sec

The drag coefficient depends on the shape and surface roughness of the object, the angle of attack of the flow and the Reynolds number $R = DU/\nu$, where D is the characteristic length of the object in ft. and ν the kinematic viscosity of the fluid in ft^2/sec. The value of C_D can be obtained analytically only when in the region of low Reynolds number i.e. when the flow is laminar. For large objects and/or high flow velocities, the flow becomes turbulent and values of C_D are best obtained by conducting scale model tests in Laboratory flumes or wind tunnels. Many such tests have been made in the past and curves of C_D vs R have been established from the test data for many basic geometric shapes in the Reynolds number range from near zero to 10^7.

Therefore, Equation (1) has been used widely to estimate drag forces with empirical values of C_D. Drag forces caused by surface wind or underwater currents can be calculated from Equation (1) using a mean wind or current velocity.

This classical drag formula is useful but is limited to constant velocity flow only. For oscillatory flow or flow in the surface wave zone, the Morison equation for piles is widely used.[3] It has an additional term to account for the inertia component of the total wave induced drag

$$P = C_D\, D\, \frac{\rho v |v|}{2} + C_I\, \frac{\pi D^2}{4}\, \rho a \qquad (2)$$

where, P = local wave force per unit length, lb/ft
D = diameter of pile, ft.
v = horizontal component of water particle velocity, ft/sec
a = horizontal component of water particle acceleration, ft/sec^2
C_I = inertia coefficient

The second term at the righthand side of Equation (2) is the inertia force which is directly proportional to the local particle acceleration and to the square of the pile diameter. The inertia coefficient, C_I, is not as well-established as the drag coefficient, C_D, and it is also more difficult to measure than the drag coefficient. Since the velocity and the acceleration are 90^o out of phase in sinusoidal flow, the drag term and the inertia term are also 90^o out of phase. The total wave force is really a vectorial sum of the two components. Therefore, the magnitude of the total force will be approximately equal to the larger component when the larger component is about 2.5 times the smaller component[3]. In cases where the drag force dominates the wave force, Equation (1) is valid.

The peak force per unit pile length at any point along the pile is

$$P = C_D \, D \, \rho \, \frac{V^2}{2}$$

where, V = peak local velocity, ft/sec

Therefore, the total peak wave force on the pile is

$$F = \int_0^L P dl = C_D \, \rho \, \frac{D}{2} \int_0^L V^2 dl$$

or

$$F = C_D \, \rho \, \frac{DL}{2} \, \overline{V^2} \tag{3}$$

where, $\overline{V^2}$ = mean square of peak velocity over the pile length

This peak force occurs when the horizontal components of the water particle velocities reach the peak. This corresponds to a crest or trough at the test section. Assuming the mean peak velocity square does not change as flow reverses direction, the direct wave force on the pile is

$$F_f = C_{Df} \, \rho \, \frac{DL_c}{2} \, \overline{V^2}$$

where, C_{Df} = drag coefficient at front of pile
L_c = submerged length of pile at wave crest, ft

and the reversed wave force is

$$F_r = C_{Dr} \, \rho \, \frac{DL_t}{2} \, \overline{V^2}$$

where, C_{Dr} = drag coefficient at rear of pile
L_t = submerged length of pile at wave trough, ft

The net peak force on the pile is

$$\Delta F = F_f \quad F_r = (C_{Df} \, L_c - C_{Dr} \, L_t) \, \frac{\rho D \overline{V^2}}{2} \tag{4}$$

Now, if the pile is very long compared to the wave height, the submerged pile length at crest may be considered equal to the length at trough and Equation (4) is reduced to

$$\Delta F = (C_{Df} - C_{Dr}) \, \frac{\rho DL \overline{V^2}}{2}$$

where, L = average submerged pile length, ft

For a symmetric pile such as a circular cylinder, $C_{Df} = C_{Dr}$ hence there is no net wave force. But a net force will be produced by a non-symmetric pile in waves. Its magnitude and direction depends upon its orientation with respect to the direction of wave propagation. For a semi-circular pile, $C_{Df} \approx 1.16$ and $C_{Dr} \approx 1.5$, when it is positioned with the curved wall facing the waves. For this case, a net force will be produced opposite to the wave direction. A similar condition results for a crescent shaped pile which will have $C_{Df} \approx 1.20$ and $C_{Dr} \approx 2.3$ when the convex side faces the waves. If these piles are rotated 180°, net forces in the direction of wave travel would be generated.

PRELIMINARY TESTS - DRIFT OBSERVATIONS

The objective of the preliminary test was to determine whether a quantitative model test with more elaborate measurements was necessary to verify or to contradict the hypothesis of producing net wave forces by non-symmetric cylinders.

The preliminary model test contained a series of drift speed observations of small scale model platforms in waves of various heights and frequencies. Circular and non-symmetric leg cross-sections were tested. By observing the speed and direction of the drift of these models, the relative magnitude of net wave forces and their direction could be determined quantitatively.

Three models were built. Each consisted of three vertical cylinders 8 inches long connected by metal bars forming an equilateral triangle with 6 inch sides. The cross-sections of the three models were circular, semicircular and crescent in shape (Figures 1, 2, and 3). Each leg was carved out of a 1-inch diameter wood dowel. The legs were ballasted to give about 2 inches of free board (Figure 4). The wave tank was 18 inches wide, 36 inches deep, and about 100 feet long. A wave generator was located at one end of the tank and created waves of small amplitude and low frequency. A solid beach, about 70 feet from the wave generator, absorbed the waves. Wave profile observation was possible through a glass wall near the middle of the wave tank. A point gauge was used to measure the wave amplitude. The drifting velocity of the platform was calculated from the time recorded for the platform to traverse a prescribed distance in the tank. Five geometries were tested for each wave as shown in Figure 5. The test wave properties and measured drift velocities were tabulated in Table 1.

Since the floating model is in a dynamic flow condition, the test results can be presented in the form of dynamic response curves. The wave frequency, f, is non-dimensionalized by the natural pitching frequency of the model, f_n. The drift velocity, V_d, is divided by the maximum peak particle velocity, V_m, to form another non-dimensional quantity.

The natural pitching frequencies of the three platform models were measured in still water by inducing free pitching oscillations. The measured values are approximately 0.8 Hz for the circular legged model with least damping, 0.83 Hz for the semicircular model and 0.62 Hz for the crescent shaped model with heaviest fluid damping.

Table 1. Results of Platform Drift Tests

Test Geometry	Natural Frequency	Wave Length	Wave Frequency	Wave Amplitude	Maximum Particle Velocity	Model Drift Velocity	Frequency Ratio	Velocity Ratio
	f_n (Hz)	λ (in)	f (Hz)	$\frac{H}{2}$ (in)	V_m (ft/sec)	V_d (ft/sec)	f/f_n	V_d/V_m
1	0.800	20	1.73	0.73	0.662	0.084	2.16	0.127
2	0.833	20	1.73	0.73	0.662	0.120	2.08	0.182
3	0.833	20	1.73	0.73	0.662	0.075	2.08	0.113
4	0.622	20	1.73	0.73	0.662	0.116	2.78	0.251
5	0.622	20	1.73	0.73	0.662	0.058	2.78	0.088
1	0.800	20	1.73	0.73	0.662	0.088	2.16	0.132
2	0.833	20	1.73	0.73	0.662	0.121	2.08	0.183
3	0.833	20	1.73	0.73	0.662	0.085	2.08	0.129
4	0.622	20	1.73	0.73	0.662	0.171	2.78	0.258
5	0.622	20	1.73	0.73	0.662	0.057	2.78	0.086
1	0.800	14	2.08	0.87	0.948	0.118	2.60	0.125
2	0.833	14	2.08	0.87	0.948	0.151	2.50	0.159
3	0.833	14	2.08	0.87	0.948	0.097	2.50	0.103
4	0.622	14	2.08	0.87	0.948	0.210	3.34	0.222
5	0.622	14	2.08	0.87	0.948	0.070	3.34	0.074
1	0.800	14	2.08	0.87	0.948	0.115	2.60	0.121
2	0.833	14	2.08	0.87	0.948	0.142	2.50	0.150
3	0.833	14	2.08	0.87	0.948	0.087	2.50	0.092
4	0.622	14	2.08	0.87	0.948	0.197	3.34	0.208
5	0.622	14	2.08	0.87	0.948	0.071	3.34	0.075

Table 1. (continued)

Test Geometry	Natural Frequency	Wave Length	Wave Frequency	Wave Amplitude	Maximum Particle Velocity	Model Drift Velocity	Frequency Ratio	Velocity Ratio
	f_n (Hz)	λ (in)	f (Hz)	$\frac{H}{2}$ (in)	V_m (ft/sec)	V_d (ft/sec)	f/f_n	V_d/V_m
1	0.800	125	0.69	1.25	0.452	0.0288	0.863	0.064
2	0.833	125	0.69	1.25	0.452	0.0411	0.831	0.091
3	0.833	125	0.69	1.25	0.452	0.0253	0.831	0.056
4	0.622	125	0.69	1.25	0.452	0.0383	1.109	0.085
5	0.622	125	0.69	1.25	0.452	0	1.109	0
1	0.800	125	0.69	1.25	0.452	0.0378	0.863	0.084
2	0.833	125	0.69	1.25	0.452	0.0418	0.831	0.093
3	0.833	125	0.69	1.25	0.452	0.0337	0.831	0.075
4	0.622	125	0.69	1.25	0.452	0.0413	1.109	0.091
5	0.622	125	0.69	1.25	0.452	0	1.109	0
1	0.800	218	0.525	0.91	0.250	0.0117	0.656	0.047
2	0.833	218	0.525	0.91	0.250	0.0095	0.633	0.038
3	0.833	218	0.525	0.91	0.250	0.0001	0.633	0.001
4	0.622	218	0.525	0.91	0.250	0.0190	0.844	0.076
5	0.622	218	0.525	0.91	0.250	0.0001	0.844	0.001
1	0.800	60	1.01	0.625	0.333	0.077	1.263	0.233
2	0.833	60	1.01	0.625	0.333	0.045	1.216	0.136
3	0.833	60	1.01	0.625	0.333	0.050	1.216	0.152
4	0.622	60	1.01	0.625	0.333	0.039	1.629	0.118
5	0.622	60	1.01	0.625	0.333	0.028	1.629	0.085
1	0.800	60	1.01	0.625	0.333	0.067	1.263	0.203
2	0.833	60	1.01	0.625	0.333	0.039	1.216	0.118
3	0.833	60	1.01	0.625	0.333	0.043	1.216	0.130
4	0.622	60	1.01	0.625	0.333	0.036	1.629	0.109
5	0.622	60	1.01	0.625	0.333	0.023	1.629	0.067

Table 1. (continued)

Test Geometry	Natural Frequency	Wave Length	Wave Frequency	Wave Amplitude	Maximum Particle Velocity	Model Drift Velocity	Frequency Ratio	Velocity Ratio
	f_n (Hz)	λ (in)	f (Hz)	$\frac{H}{2}$ (in)	V_m (ft/sec)	V_d (ft/sec)	f/f_n	V_d/V_m
1	0.800	60	1.01	0.625	0.333	0.067	1.263	0.203
2	0.833	60	1.01	0.625	0.333	0.039	1.216	0.118
3	0.833	60	1.01	0.625	0.333	0.045	1.216	0.136
4	0.622	60	1.01	0.625	0.333	0.036	1.629	0.109
5	0.622	60	1.01	0.625	0.333	0.025	1.629	0.076
1	0.800	60	1.01	1.0	0.528	0.150	1.263	0.284
2	0.833	60	1.01	1.0	0.528	0.083	1.216	0.157
3	0.833	60	1.01	1.0	0.528	0.066	1.216	0.125
4	0.622	60	1.01	1.0	0.528	0.084	1.629	0.159
5	0.622	60	1.01	1.0	0.528	0.048	1.629	0.091
1	0.800	60	1.01	1.0	0.528	0.133	1.263	0.252
2	0.833	60	1.01	1.0	0.528	0.074	1.216	0.140
3	0.833	60	1.01	1.0	0.528	0.063	1.216	0.119
4	0.622	60	1.01	1.0	0.528	0.083	1.629	0.157
5	0.622	60	1.01	1.0	0.528	0.040	1.629	0.075
1	0.800	60	1.01	1.0	0.528	0.136	1.263	0.257
2	0.833	60	1.01	1.0	0.528	0.080	1.216	0.151
3	0.833	60	1.01	1.0	0.528	0.068	1.216	0.129
4	0.622	60	1.01	1.0	0.528	0.090	1.629	0.170
5	0.622	60	1.01	1.0	0.528	0.048	1.629	0.091
1	0.800	36	1.31	0.625	0.428	0.079	1.638	0.185
2	0.833	36	1.31	0.625	0.428	0.072	1.578	0.168
3	0.833	36	1.31	0.625	0.428	0.058	1.578	0.136
4	0.622	36	1.31	0.625	0.428	0.084	2.112	0.196
5	0.622	36	1.31	0.625	0.428	0.040	2.112	0.093

Table 1. (continued)

Test Geometry	Natural Frequency	Wave Length	Wave Frequency	Wave Amplitude	Maximum Particle Velocity	Model Drift Velocity	Frequency Ratio	Velocity Ratio
	f_n (Hz)	λ (in)	f (Hz)	$\frac{H}{2}$ (in)	V_m (ft/sec)	V_d (ft/sec)	f/f_n	V_d/V_m
1	0.800	36	1.31	0.625	0.428	0.087	1.638	0.203
2	0.833	36	1.31	0.625	0.428	0.063	1.578	0.147
3	0.833	36	1.31	0.625	0.428	0.052	1.578	0.121
4	0.622	36	1.31	0.625	0.428	0.073	2.112	0.171
5	0.622	36	1.31	0.625	0.428	0.041	2.112	0.096
1	0.800	36	1.31	0.625	0.428	0.087	1.638	0.203
2	0.833	36	1.31	0.625	0.428	0.056	1.578	0.131
3	0.833	36	1.31	0.625	0.428	0.055	1.578	0.129
4	0.622	36	1.31	0.625	0.428	0.070	2.112	0.164
5	0.622	36	1.31	0.625	0.428	0.041	2.112	0.096
1	0.800	36	1.31	1.0	0.686	0.150	1.638	0.219
2	0.833	36	1.31	1.0	0.686	0.140	1.578	0.204
3	0.833	36	1.31	1.0	0.686	0.083	1.578	0.121
4	0.622	36	1.31	1.0	0.686	0.162	2.112	0.236
5	0.622	36	1.31	1.0	0.686	0.063	2.112	0.092
1	0.800	36	1.31	1.0	0.686	0.158	1.638	0.230
2	0.833	36	1.31	1.0	0.686	0.131	1.578	0.191
3	0.833	36	1.31	1.0	0.686	0.095	1.578	0.138
4	0.622	36	1.31	1.0	0.686	0.164	2.112	0.239
5	0.622	36	1.31	1.0	0.686	0.074	2.112	0.108
1	0.800	25	1.57	0.625	0.514	0.072	1.963	0.140
2	0.833	25	1.57	0.625	0.514	0.084	1.891	0.163
3	0.833	25	1.57	0.625	0.514	0.060	1.891	0.117
4	0.622	25	1.57	0.625	0.514	0.111	2.532	0.216
5	0.622	25	1.57	0.625	0.514	0.039	2.532	0.076

Table 1. (continued)

Test Geometry	Natural Frequency	Wave Length	Wave Frequency	Wave Amplitude	Maximum Particle Velocity	Model Drift Velocity	Frequency Ratio	Velocity Ratio
	f_n (Hz)	λ (in)	f (Hz)	$\frac{H}{2}$ (in)	V_m (ft/sec)	V_d (ft/sec)	f/f_n	V_d/V_m
1	0.800	25	1.57	0.625	0.514	0.060	1.963	0.117
2	0.833	25	1.57	0.625	0.514	0.080	1.891	0.156
3	0.833	25	1.57	0.625	0.514	0.063	1.891	0.123
4	0.622	25	1.57	0.625	0.514	0.113	2.532	0.220
5	0.622	25	1.57	0.625	0.514	0.043	2.532	0.084
1	0.800	25	1.57	1.0	0.822	0.140	1.963	0.170
2	0.833	25	1.57	1.0	0.822	0.153	1.891	0.186
3	0.833	25	1.57	1.0	0.822	0.102	1.891	0.124
4	0.622	25	1.57	1.0	0.822	0.187	2.532	0.227
5	0.622	25	1.57	1.0	0.822	0.095	2.532	0.116
1	0.800	25	1.57	1.0	0.822	0.132	1.963	0.160
2	0.833	25	1.57	1.0	0.822	0.144	1.891	0.175
3	0.833	25	1.57	1.0	0.822	0.109	1.891	0.133
4	0.622	25	1.57	1.0	0.822	0.179	2.532	0.218
5	0.622	25	1.57	1.0	0.822	0.083	2.532	0.101
1	0.800	15	2.02	0.187	0.198	0.0215	2.525	0.108
2	0.833	15	2.02	0.187	0.198	0.0245	2.433	0.124
3	0.833	15	2.02	0.187	0.198	0.0180	2.433	0.141
4	0.622	15	2.02	0.187	0.198	0.0385	3.258	0.194
5	0.622	15	2.02	0.187	0.198	0.0130	3.258	0.065
1	0.800	15	2.02	0.187	0.198	0.0220	2.525	0.222
2	0.833	15	2.02	0.187	0.198	0.0245	2.433	0.247
3	0.833	15	2.02	0.187	0.198	0.0210	2.433	0.212
4	0.622	15	2.02	0.187	0.198	0.0375	3.258	0.379
5	0.622	15	2.02	0.187	0.198	0.0135	3.258	0.136

Table 1. (conclusion)

Test Geometry	Natural Frequency	Wave Length	Wave Frequency	Wave Amplitude	Maximum Particle Velocity	Model Drift Velocity	Frequency Ratio	Velocity Ratio
	f_n (Hz)	λ (in)	f (Hz)	$\frac{H}{2}$ (in)	V_m (ft/sec)	V_d (ft/sec)	f/f_n	V_d/V_m
1	0.800	12	2.26	0.625	0.740	0.068	2.825	0.092
2	0.833	12	2.26	0.625	0.740	0.070	2.723	0.095
3	0.833	12	2.26	0.625	0.740	0.057	2.723	0.077
4	0.622	12	2.26	0.625	0.740	0.103	3.645	0.139
5	0.622	12	2.26	0.625	0.470	0.039	3.645	0.053
1	0.800	13	2.17	0.625	0.710	0.069	2.713	0.097
2	0.833	13	2.17	0.625	0.710	0.077	2.614	0.108
3	0.833	13	2.17	0.625	0.710	0.065	2.614	0.092
4	0.622	13	2.17	0.625	0.710	0.118	3.500	0.166
5	0.622	13	2.17	0.625	0.710	0.056	3.500	0.079

The response curves of the circular, semi-circular, and crescent shaped models are shown in Figures 6, 7, and 8, respectively. One would expect a peak response when the wave frequency matched the platform's natural pitch frequency. But the responses of all three platform models peaked at wave frequencies higher than the natural frequencies. The circular cylinder platform has a wide spread of data points (Figure 6). Unfortunately, the peak of the response curve cannot be defined because of the lack of data points near $f/f_n = 1$. However, the peak responses of the non-symmetric legged platforms fall definitely beyond $f/f_n = 1$. This indicates that the model resonance frequencies are different from the natural pitch frequencies of models measured in still water.

All five response curves were replotted on Figure 9 for comparison. In general, all tests resulted in "downstream" drifts. However, there is a trend that indicates "upstream" platform motion can be achieved in low frequency waves. The velocity of such drift, however, is not significant. Upstream drift was observed in very long waves for several unrecorded tests in which the drift velocities were too small to be recorded.

The dimensionless drift velocity, V_d/V_m, measures the efficiency of each test geometry in converting wave energy into propulsion force. The ranking with respect to peak values of drift velocity are; test geometry 4 the highest, geometry 1 the second, and geometry 2, 3, and 5 the third, fourth and fifth, respectively. Based on the hypothesis discussed in the background section, the drift velocities for geometry 2 and 4 were expected to be high and drifts against wave direction were predicted for geometries 3 and 5. The circular model was expected to be stationary. The high velocity of geometry 4 and some upstream drift in geometry 5 have somewhat confirmed the theory. The high velocity drift of the circular model and the failure of upstream drift by geometry 3 indicate that some force other than the hydrodynamic drag force possibly the inertia force predominated the wave force.

These results have indicated that non-symmetric platform legs may provide definite advantages over the conventional circular legs. Further investigation was therefore justified. The next step was to conduct a more elaborate model test to measure the peak wave forces on larger models for more effective evaluation of non-symmetric leg geometries.

PRINCIPAL TESTS - WAVE FORCE MEASUREMENTS

Three different models of a MOBS platform leg, 1 to 60 scale in length were fabricated from 4-inch and 6-inch PVC pipes. The length of each model was 8 feet long. Again, a circular, a semi-circular, and a crescent shaped cross-section were selected for these models. The dimensions of model sections are shown in Figure 10. A base plate and stiffening collar were attached at the upper end of each model for easier and faster mounting and removal from the support.

The model tests were conducted in the Ocean Laboratory of the Offshore Technology Corporation, Escondido, California. The test tank resembled a deep swimming pool 50 feet wide, 150 feet long, and 15 feet deep (Figure 11).

At one end of the tank, there was a hinged wave generator powered by two hydraulic cylinders. Wave form, height, length, period can be readily varied. Maximum wave height is approximately 12 inches. At the other end of the tank were three layers of wave absorbers to minimize wave reflection. An observation window is installed at the side wall at the test section near the middle of the tank. At this same location, a portable truss was positioned across the tank. The truss provided a mounting support for the models and wave gauges. The models were fastened to aluminum plates suspended from the bottom members of the truss by four steel rods. These rods are notched to provide the models with freedom of horizontal movement. Three models were mounted near the center of the tank along the testing section about three feet apart (Figure 12). Wave forces on each model at directions parallel and normal to the waves were measured by two sets of springs instrumented with two strain gauges. These springs were supported by four rods fixed rigidly to the truss (Figures 13 and 14). A wave staff was mounted at the test section in line with the models. The wave gauge output together with six strain gauge outputs were conditioned and displayed on a multi-channel oscillogram. These signals were also recorded on a magnetic tape recorder.

Wave force measurements were obtained for waves having a wide range of wave height, wave length, and the height to length ratio. Table 2 is a summary of designed testing waves.

A trial and error technique was necessary to adjust the wave properties closer to values in Table 2. However, it is almost impossible to adjust the wave height to a preset value. The actual wave measurements are listed together with the test results in Table 3.

Models were tested in three different orientations. They were first mounted so that the flat side of the semi-circular model and the concave side of the crescent shaped model were facing the impinging waves. The second mounting orientation was 90^{o} from the first orientation and the third was 180^{o} from the first. About twenty wave trains were tested in each model orientation.

Wave staff and wave force gauges were carefully calibrated before the test started and the calibrations were checked after each series of tests were completed. To calibrate force gauges, weights of one pound increment were attached through a pulley system to the model mounting plates. Negative wave forces were simulated by hanging weights at the upstream side of the mounting.

Oscillogram records were reduced by measuring the positive and the negative peak forces averaged over five or six waves. No attempt was made to analyze the wave forms.

A samples of the oscillogram recordings is shown in Figure 15. Higher frequency vibration noises are visible in the traces of wave forces. As the lowest vibration frequency (crescent model) is about ten times higher than the wave frequency, the effects of the noise signals can be eliminated easily. In most records the noise level was relatively small.

Table 2. Design Waves for Wave Force Measurement Tests

Run No.	Wave Height		Wave Length		Height / Length
	Model	Prototype	Model	Prototype	
	in	ft	ft	ft	
1	2	10	4	240	0.042
2			6	360	0.028
3			8	480	0.021
4			12	720	0.014
5	4	20	6	360	0.056
6			8	480	0.042
7			12	720	0.028
8			15	900	0.022
9	6	30	8	480	0.063
10			12	720	0.042
11			15	900	0.033
12			20	1200	0.025
13	8	40	12	720	0.056
14			15	900	0.045
15			20	1200	0.033
16			30	1800	0.022
17	12	60	15	900	0.067
18			20	1200	0.050
19			30	1800	0.033

Table 3. Result of Wave Force Measurements

Test No.	Wave Height	Wave Length	Height / Length	Circular		Circular	Semi-circular		Semi-circular	Crescent		Crescent
				Peak Forces		Phase Lag	Peak Forces		Phase Lag	Peak Forces		Phase Lag
	H (in)	λ (ft)	$\frac{H}{\lambda}$	F_1 (lb)		θ_1 (degree)	F_2 (lb)		θ_2 (degree)	F_3 (lb)		θ_3 (degree)
101	2.0	4	0.042	1.1	-2.0	180	0.9	-0.7	98	1.1	-0.9	88
102	2.2	6	0.031	4.5	-5.1	88	0.8	-0.6	230	0.7	-0.7	88
103	2.4	8	0.025	1.7	-2.8	95	2.0	-1.9	189	0.2	-0.5	128
104	1.8	12	0.013	1.7	-1.8	90	2.4	-1.8	122	2.1	-1.2	165
105	4.0	6	0.056	6.9	-7.0	80	2.1	-1.2	205	2.5	-1.5	120
106	4.2	8	0.044	3.9	-3.0	65	3.3	-2.5	180	1.5	-0.9	110
107	5.6	12	0.039	4.3	-4.8	85	5.5	-4.5	150	4.5	-2.8	160
108	3.7	12	0.026	2.7	-2.5	85	3.5	-3.0	125	2.8	-2.0	160
109	3.9	15	0.022	2.2	-4.0	65	3.0	-2.6	135	3.5	-2.2	140
110	5.6	8	0.058	4.8	-4.5	70	4.2	-3.8	165	2.8	-1.5	120
111	----	--	-----	---	----	---	---	----	---	---	----	---
112	6.9	20	0.029	5.1	-4.0	65	6.2	-5.2	110	7.1	-5.5	150
113	11.6	20	0.048	6.7	-7.8	60	13.0	-7.8	130	12.0	-7.7	155
114	8.4	12	0.058	5.5	-6.5	70	7.1	-3.5	135	5.3	-4.0	145
115	7.6	20	0.032	5.0	-4.2	60	7.6	-5.6	140	7.4	-5.9	155
116	7.6	30	0.021	4.4	-3.6	55	5.8	-3.6	115	6.1	-5.0	125
117	9.9	30	0.028	5.0	-5.1	60	7.5	-5.5	125	8.2	-6.1	135
118	13.0	30	0.036	6.3	-6.6	60	8.8	-7.2	115	11.8	-8.0	130
NOTE: High drag side of models toward wave.												
201	2.2	4	0.046	3.1	-1.6	135	---	----	---	---	----	---
202	1.9	6	0.025	2.1	-2.0	60	---	----	---	---	----	---
203	2.2	8	0.022	1.8	-1.8	70	---	----	---	---	----	---
204	2.1	12	0.015	1.6	-1.6	75	---	----	---	---	----	---
205	4.5	6	0.063	5.4	-6.5	65	---	----	---	---	----	---
206	3.9	6	0.054	4.4	-5.5	75	---	----	---	---	----	---
207	4.4	8	0.046	4.2	-4.0	65	---	----	---	---	----	---
208	3.9	12	0.027	2.8	-3.2	85	---	----	---	---	----	---
209	3.7	15	0.021	2.9	-4.1	75	---	----	---	---	----	---
210	6.3	8	0.067	6.8	-6.0	75	---	----	---	---	----	---

Table 3. (cont'd)

Test No.	Wave Height	Wave Length	Height / Length	Circular			Semi-circular			Crescent		
				Peak Forces		Phase Lag	Peak Forces		Phase Lag	Peak Forces		Phase Lag
	H (in)	λ (ft)	$\frac{H}{\lambda}$	F_1 (lb)		θ_1 (degree)	F_2 (lb)		θ_2 (degree)	F_3 (lb)		θ_3 (degree)
211	7.8	12	0.054	6.4	-7.2	80	---	----	---	---	----	---
212	5.7	12	0.040	4.8	-5.2	75	---	----	---	---	----	---
213	6.2	20	0.026	5.2	-4.8	55	---	----	---	---	----	---
214	8.5	20	0.035	6.5	-4.7	60	---	----	---	---	----	---
215	7.2	30	0.020	5.2	-4.3	50	---	----	---	---	----	---
216	---	--	-----	---	----	--	---	----	---	---	----	---
217	8.8	30	0.024	4.9	-4.8	50	---	----	---	---	----	---
218	10.7	30	0.030	6.1	-4.9	70	---	----	---	---	----	---
219	2.2	4	0.046	6.4	-7.0	170	---	----	---	---	----	---
220	1.6	2	0.067	1.8	-2.4	210	---	----	---	---	----	---
301	2.5	3.5	0.059	4.3	-5.3	200	1.9	-1.4	40	1.6	-1.4	60
302	1.4	2.6	0.044	1.3	-1.2	0	1.0	-0.9	0	1.0	-1.0	60
303	2.0	6	0.027	1.6	-2.0	70	1.2	-1.1	185	0.6	-0.7	60
304	2.0	8	0.020	1.4	-2.0	80	2.0	-1.8	100	0.2	-0.5	160
305	2.1	12	0.014	1.3	-2.0	70	1.5	-1.5	100	1.7	-2.0	150
306	4.6	6	0.063	4.8	-5.2	70	2.4	-2.1	180	1.8	-1.2	95
307	3.4	8	0.035	3.0	-3.8	75	3.5	-3.3	140	0.9	-1.0	155
308	4.0	12	0.027	2.9	-3.6	80	3.4	-2.9	120	2.9	-2.9	160
309	3.7	15	0.020	2.7	-3.5	55	3.0	-2.5	100	3.1	-3.6	135
310	6.9	8	0.071	6.4	-6.9	85	6.5	-5.2	170	3.0	-2.5	145
311	5.9	12	0.040	4.0	-5.5	85	4.6	-4.1	125	3.4	-4.0	165
312	5.9	20	0.024	4.4	-5.5	50	3.8	-3.9	120	5.0	-5.2	140
313	7.7	12	0.053	5.3	-5.5	90	5.4	-4.9	130	4.2	-4.6	170
314	7.6	20	0.031	5.8	-5.0	65	4.9	-4.8	130	5.9	-6.6	165
315	8.8	30	0.024	4.9	-5.2	60	5.3	-4.6	120	6.6	-7.0	130
316	9.1	20	0.037	6.5	-6.5	65	7.9	-7.6	130	8.2	-9.2	160
317	10.8	30	0.030	5.4	-5.6	70	7.2	-6.3	120	7.9	-9.2	140

NOTE: Low drag side of models toward wave.

RESULTS

The results of the wave force measurements are tabulated in Table 3. The difference among 100, 200, and 300 series data is model orientation. The 100 series tests were conducted with the higher drag sides of models facing on-coming waves. The models were turned 90° for 200 series and 180° for 300 series. The values of phase lags were obtained from the oscillogram records by measuring the difference in phase angle between the wave peak and the force peak.

The objectives of the 200 series test were to observe the lift forces (force normal to flow) on the non-symmetric models and to provide more drag data on circular models. The noise to signal ratio was large in the lift force recordings of the non-symmetric models and their peak force and phase lag could not be determined accurately. Drag forces on these geometries were of little interest. Consequently, these data were not included in Table 3. A qualitative analysis of the force records of the non-symmetric models indicates that large net lift forces cannot be produced by orienting the long axis of the model cross-section in parallel to the on-coming wave direction.

The absolute values of positive (direction of wave propagation) and negative peak forces on the circular, semi-circular, and crescent shaped models are plotted against the wave steepness (ratio of wave height to length) for the 100 series tests in Figures 16, 17 and 18. A family of curves is shown in each plot with wave length as a parameter. The wave force increases with increasing wave length and wave steepness. Figure 19 shows the wave peak forces on crescent shaped model in 300 series tests. By comparing Figure 19 with Figure 18, it can be shown that the major difference is the change in signs of the wave forces. The 300 series data indicate the larger forces are negative forces whereas the 100 series data indicate the larger forces are positive forces.

The net differential peak forces, the difference between positive and negative peaks, are plotted against wave heights and are presented in Figures 20, 21, and 22 for the three models. The circular model data in Figure 20 are wide spread about a mean value of zero. The semi-circular model experiences no net negative forces in either orientation as shown in Figure 21. However, the wave forces are much smaller when the model is mounted with the circular side facing the on-coming waves. For the crescent shaped model net negative peak forces are clearly shown in Figure 22 when waves approach from the convex side. There are, however, several data points which fall about the axis. This apparent discrepancy could be caused by zero drift in the force gauge calibration which was found after the tests were completed. The spread of the rest of data is small enough to determine a mean which is sensitive to wave height.

A study of the lag angle between the peak force and the wave peak reveals whether the drag or the inertia force predominates. For a 90° or 270° lag, the wave force is in phase with the water particle acceleration and is, therefore, mainly due to inertia effects. A lag of 0° or 180° indicates the wave force is in phase with the water particle velocity, and is, therefore, controlled by drag. Figures 23, 24, and 25 are measured

phase lag angles of all the experimental data. The circular cylinder has a mean phase lag of 75° indicating a dominative inertia force. For the semi-circular model, most of the phase lags fall between 90° and 180°. Therefore, the wave force on the semi-circular model is affected by both drag and inertia forces. This is also true for the crescent shaped model. The difference between these two is that all small wave heights the semi-circular model has a higher percentage of inertia force than that for the crescent model. At the larger wave heights, the trends are reversed but the data are too scattered to give conclusive results. The inertia force is proportional to the virtual mass which increases with the amount of water displaced by the submerged object. Consequently, the trend from inertia domination for the circular model to near drag domination for the crescent model is probably due to the difference in the amount of water displaced by the models.

To convert the model data to the MOBS prototype, simply multiply the model wave height and length by the length factor of 60 and multiply the wave force by the force factor of 216,000. Notice that the net peak force is neither a constant force nor a sinusoidal force. It is recommended, therefore, that the test data be used with caution.

FINDINGS

1. For wave frequencies near the natural pitching frequency, the model platform with circular legs had the fastest drift velocity. High drift velocity over a wide frequency range was observed during tests of the platform having crescent shaped legs with waves coming at the concave side. The slowest platform was the same platform model with the convex side facing the waves. For very low frequency waves, this model was observed to move against the direction of wave propagation.

2. The frequency response of the three platforms does not follow the motion of a one degree of freedom mechanical system. The dynamically measured natural frequencies are higher than the statically measured natural pitching frequency.

3. Net negative peak wave forces were measured only on the crescent shaped platform leg model with the convex side facing the waves. These forces were relatively small and were proportional to the wave height.

4. Large net positive peak forces were measured on both crescent and semi-circular leg models with waves approaching the concave and flat sides.

5. For the test conditions, inertia force dominated the wave force on circular cylinders and drag force essentially dominated the wave force on crescent cylinders.

CONCLUSIONS OF HYDRAULIC MODEL STUDIES

1. The crescent-shaped columns can provide a limited force in the direction of wave propagation when they are oriented with the convex side facing the approaching waves. They are most effective in high waves of low frequencies.

2. The crescent-shaped columns can be also used to create maximum wave drag for propulsion purpose when they are positioned with waves coming toward the concave sides.

3. The hypothesis that differential wave forces may be produced by unsymmetrical cylinders having two different drag coefficients is valid in cases where the inertia force is insignificant.

4. No significant amount of net lift force can be produced by orienting the long axis of the cross-section of the non-symmetric models in parallel with the direction of wave propagation.

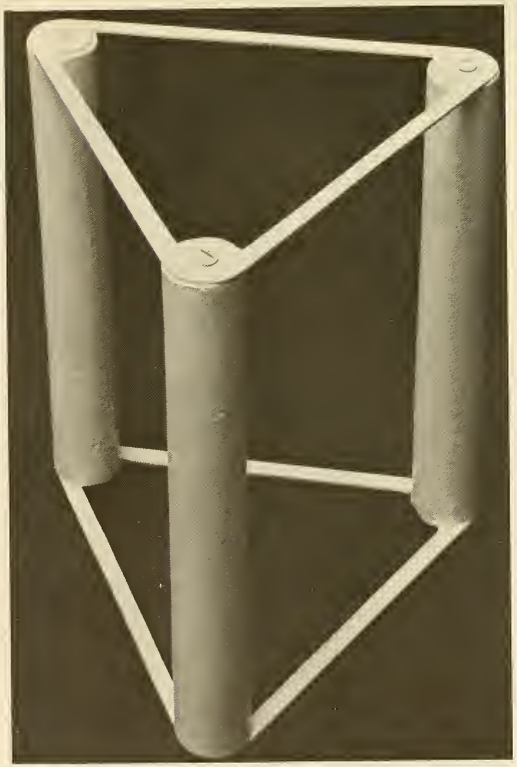

Figure 1. Floating Platform Model with Circular Legs.

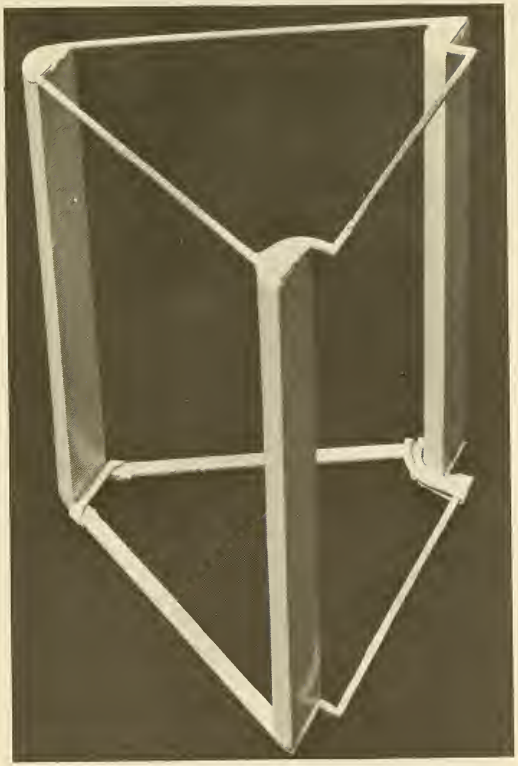

Figure 2. Floating Platform Model with Semi-circular Legs.

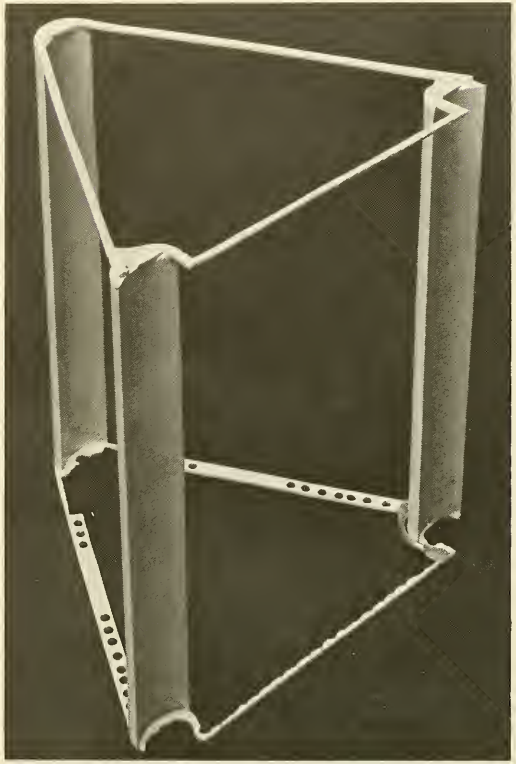

Figure 3. Floating Platform Model with Crescent Shaped Legs

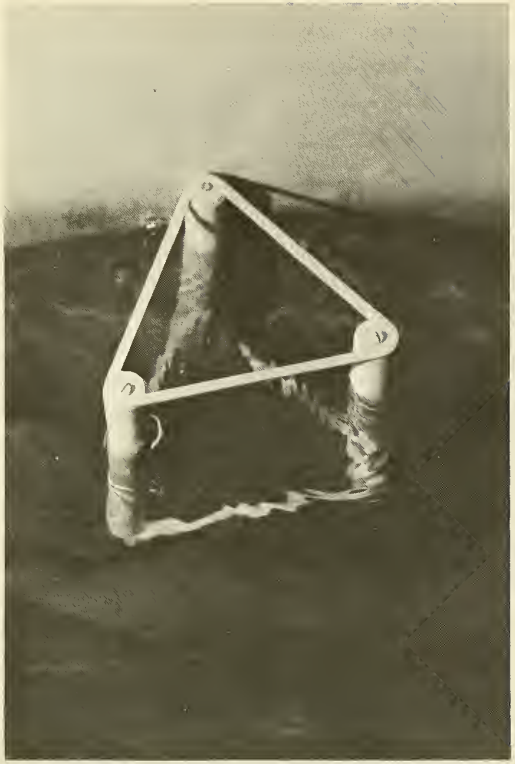

Figure 4. Circular Legged Platform Model Under Drifting Test

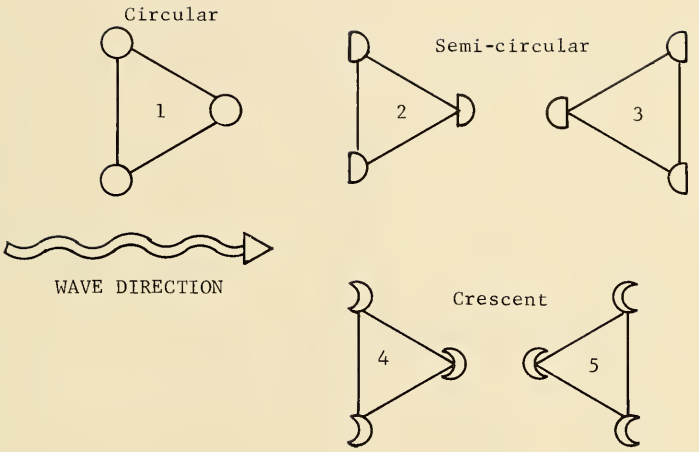

Figure 5. Model geometries for drift experiment.

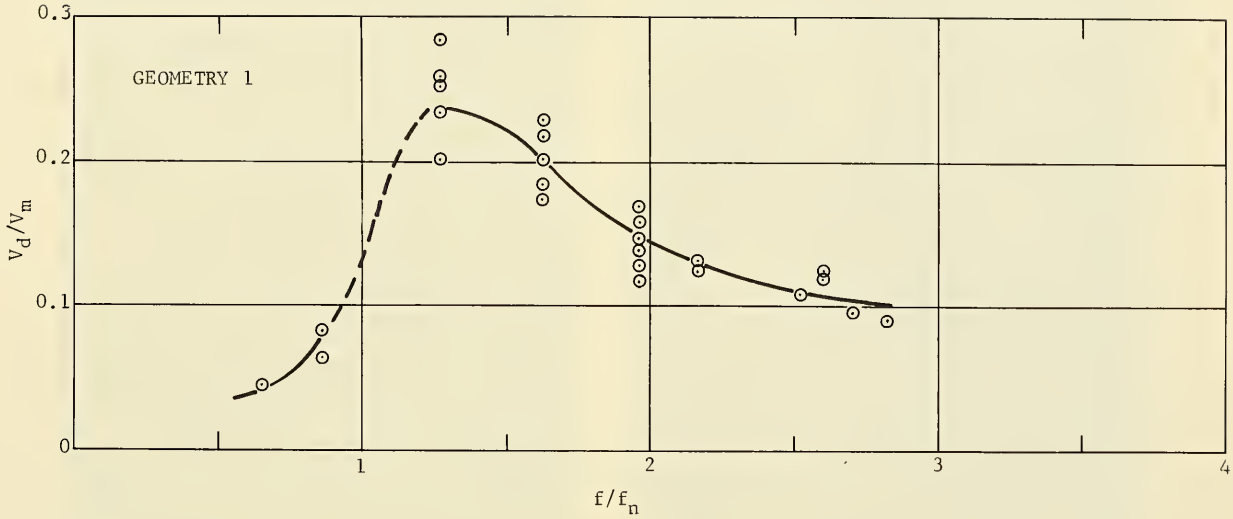

Figure 6. Dynamic response of drifting platform with circular legs

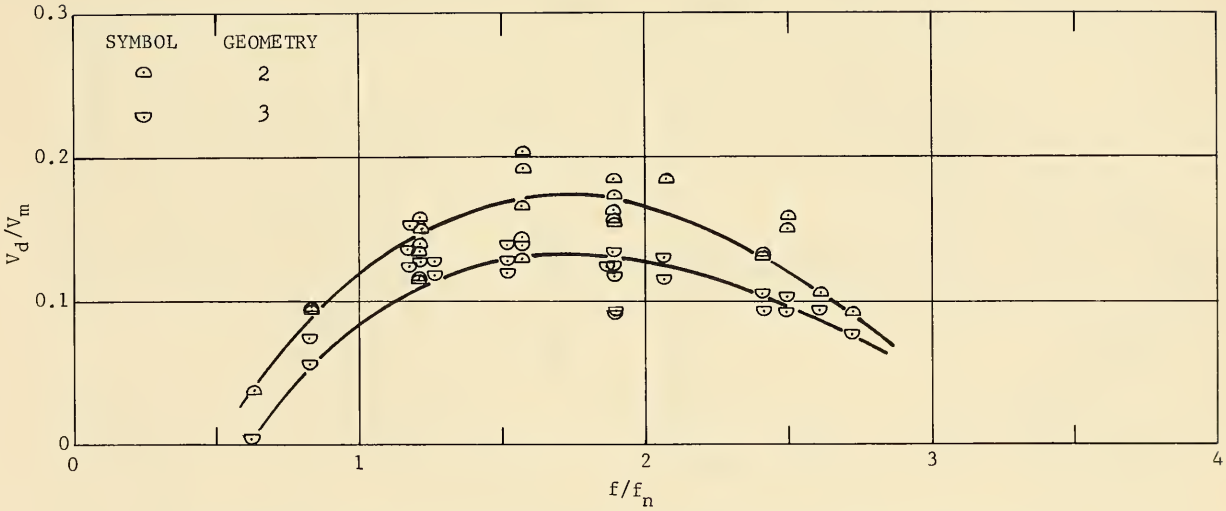

Figure 7. Dynamic response of drifting platform with semi-circular legs

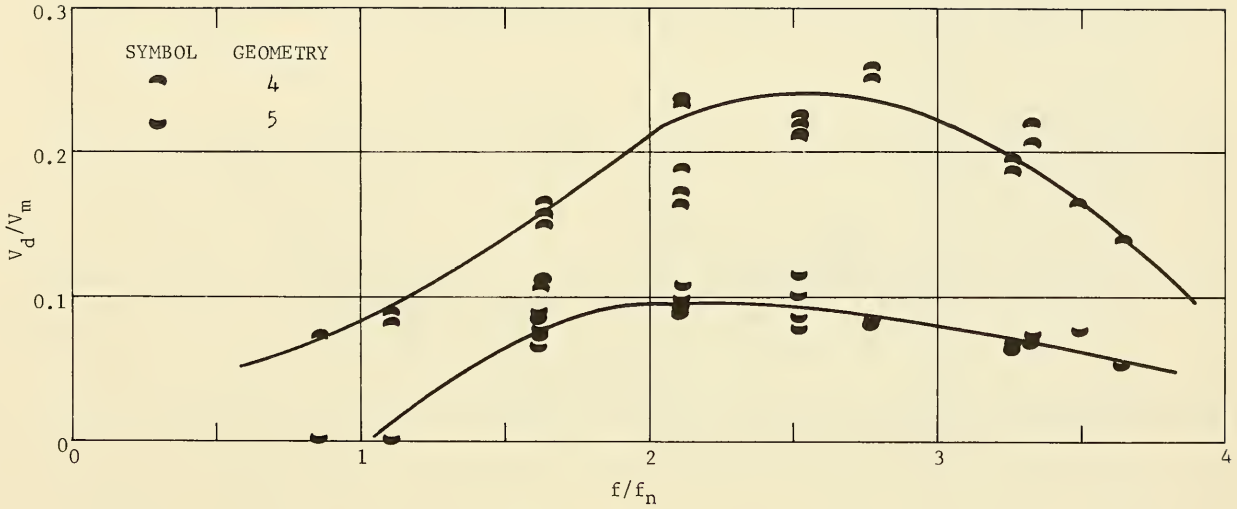

Figure 8. Dynamic response of drifting platform with crescent shaped legs

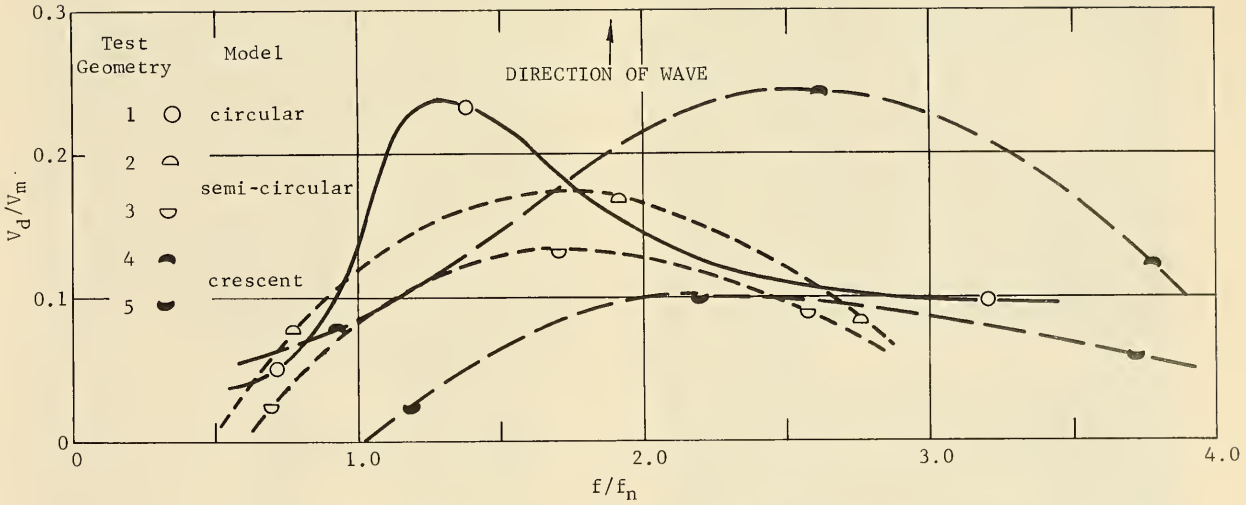

Figure 9. Comparison of the dynamic responses of three platform models

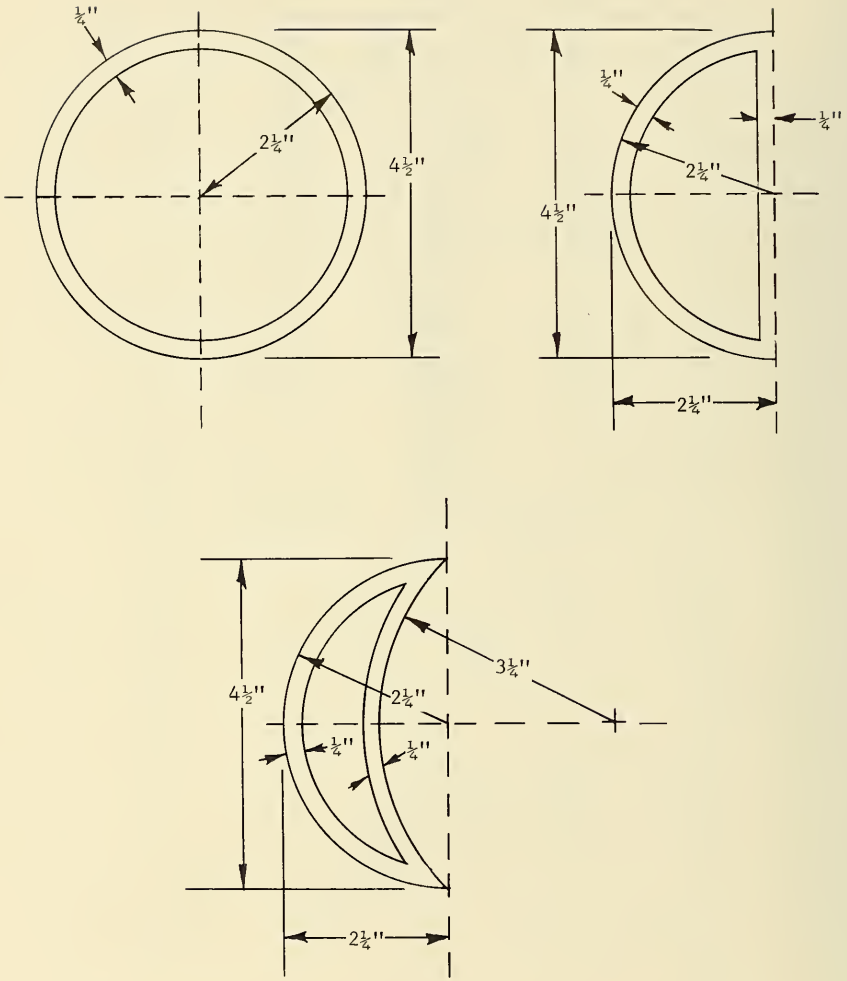

Figure 10. Cross-sections of platform leg models

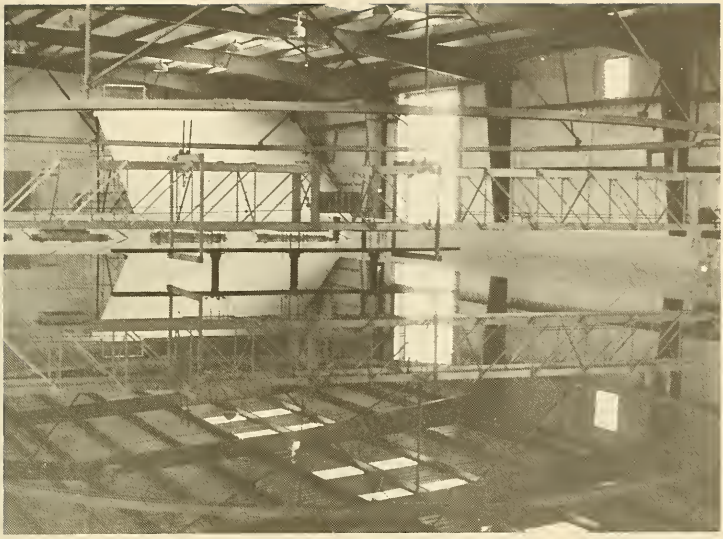

Figure 11. Wave tank facility used for the measurements of wave forces on platform leg models.

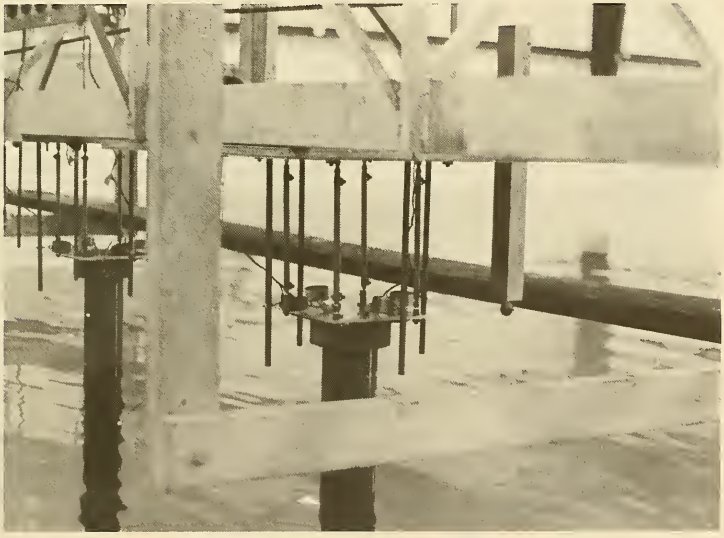

Figure 12. Platform leg models in position.

Figure 13. Wave forces in two perpendicular directions were measured by two sets of strain-gauged rings.

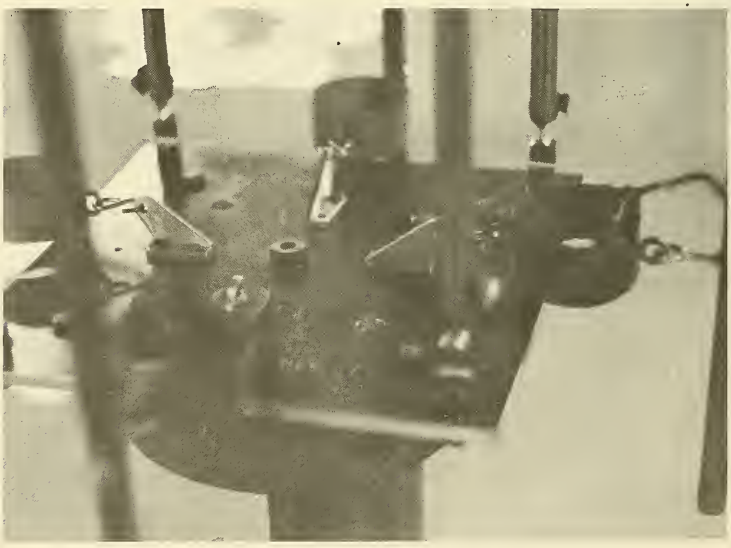

Figure 14. Close-up view of the model mounting.

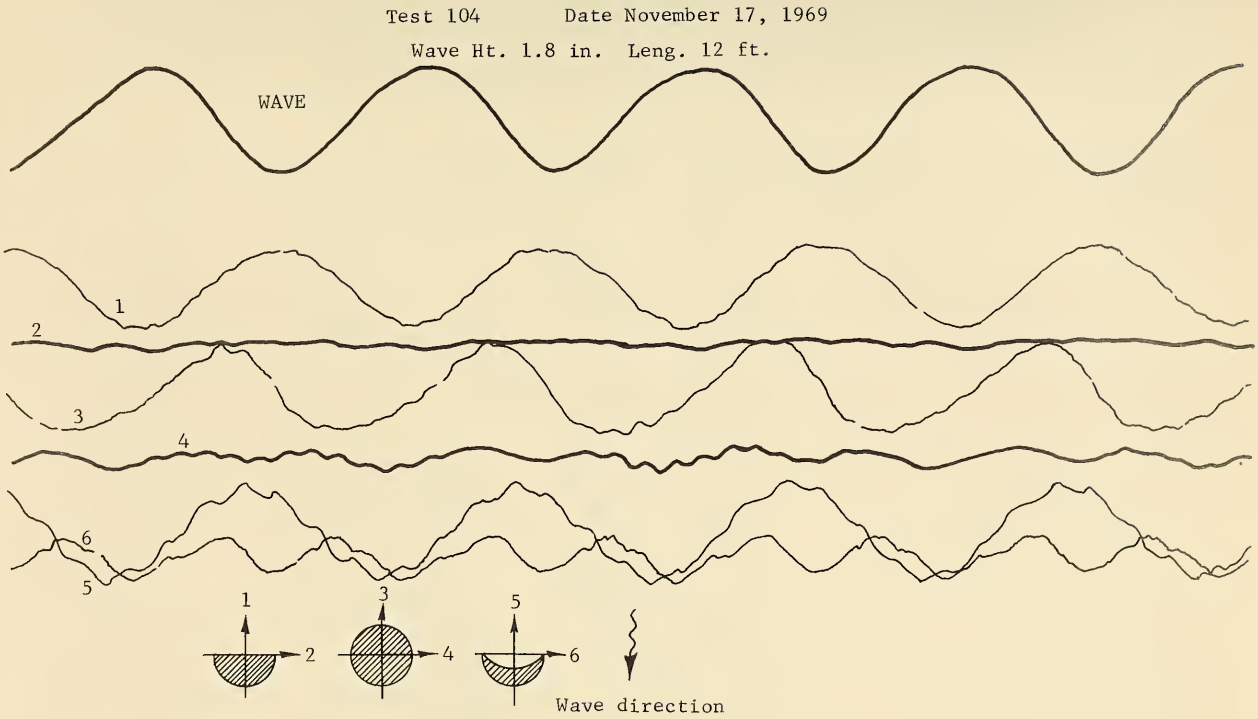

Figure 15. Oscillogram traces of wave height and forces

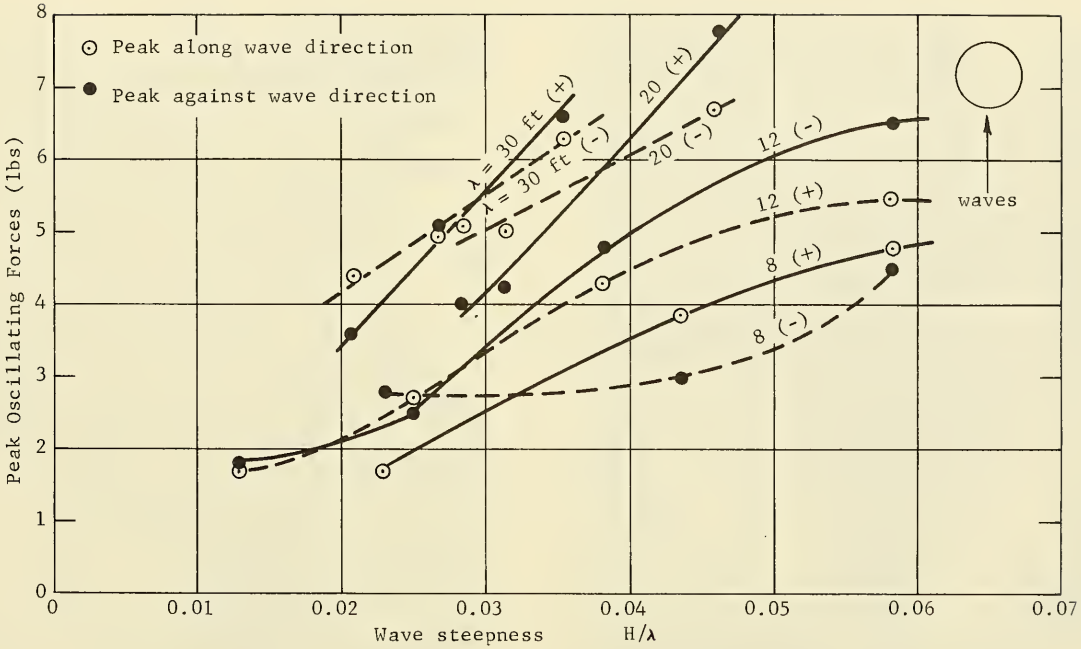

Figure 16. Wave forces on circular model - 100 series

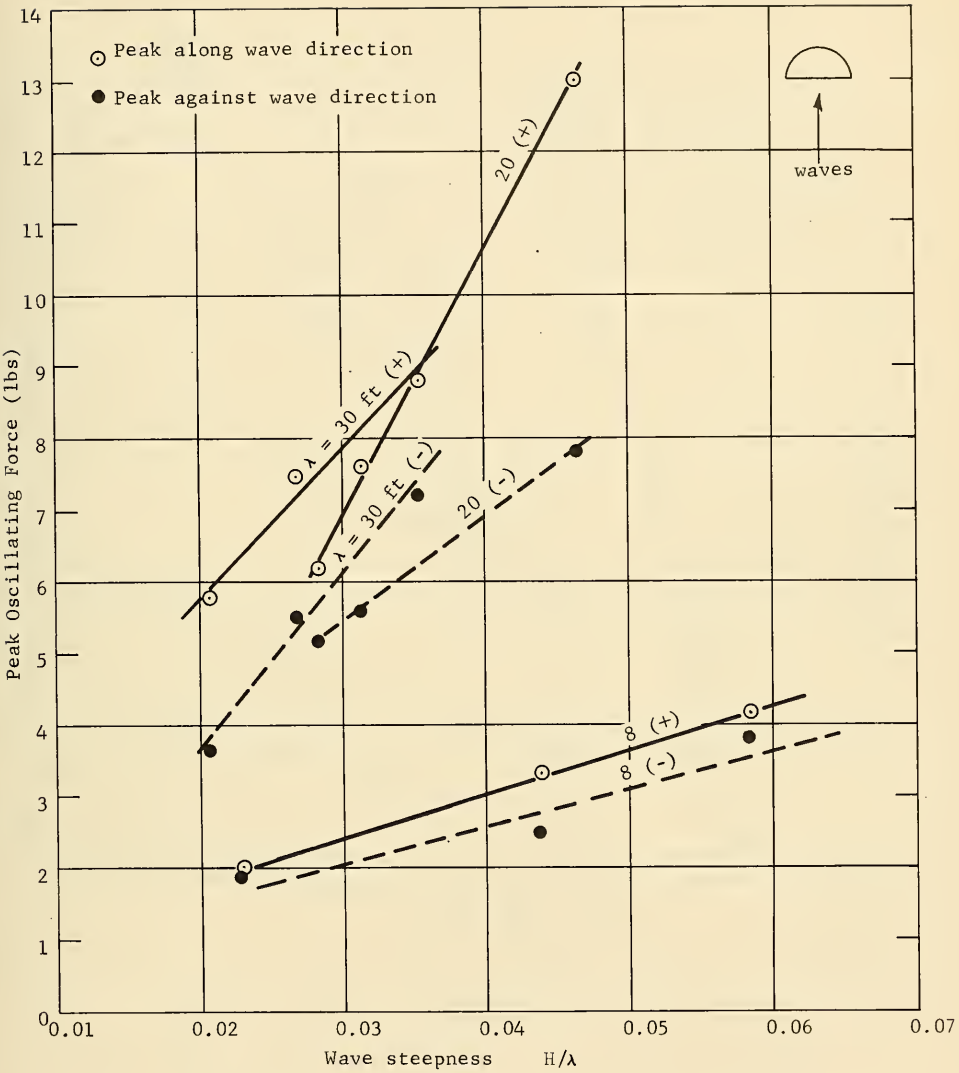

Figure 17. Wave forces on semi-circular model - 100 series.

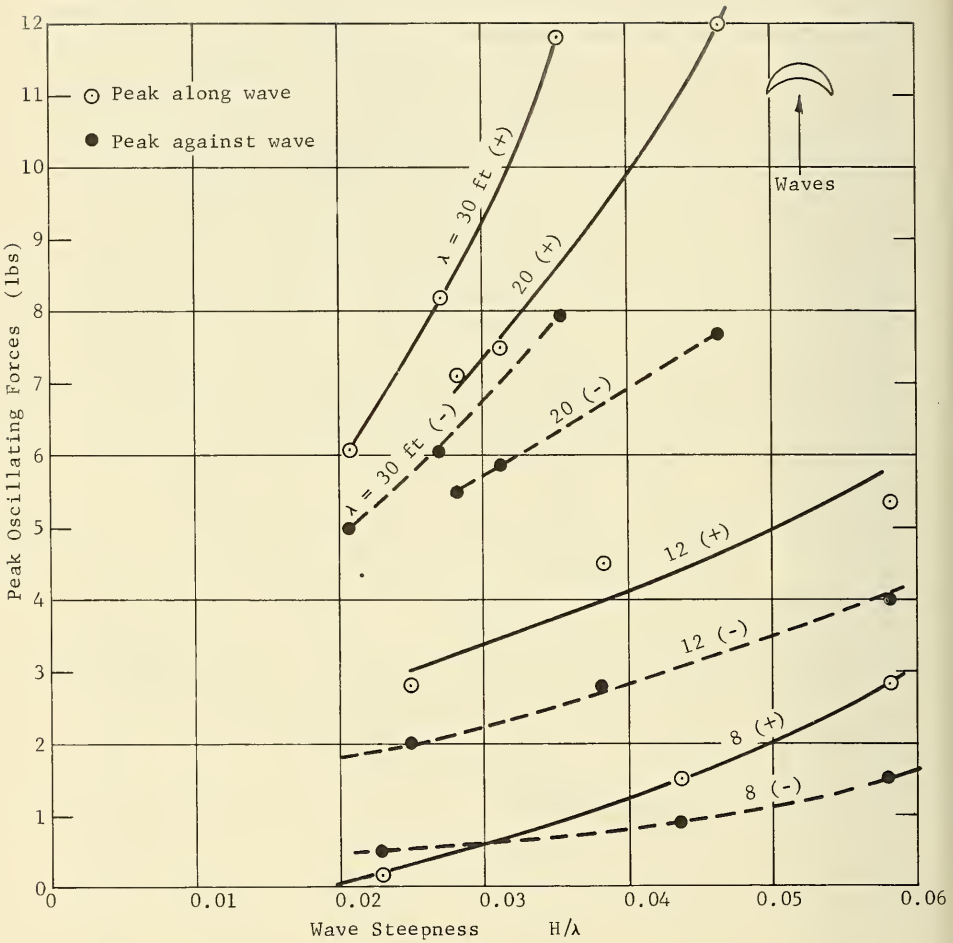

Figure 18. Wave forces on crescent shaped model - 100 series.

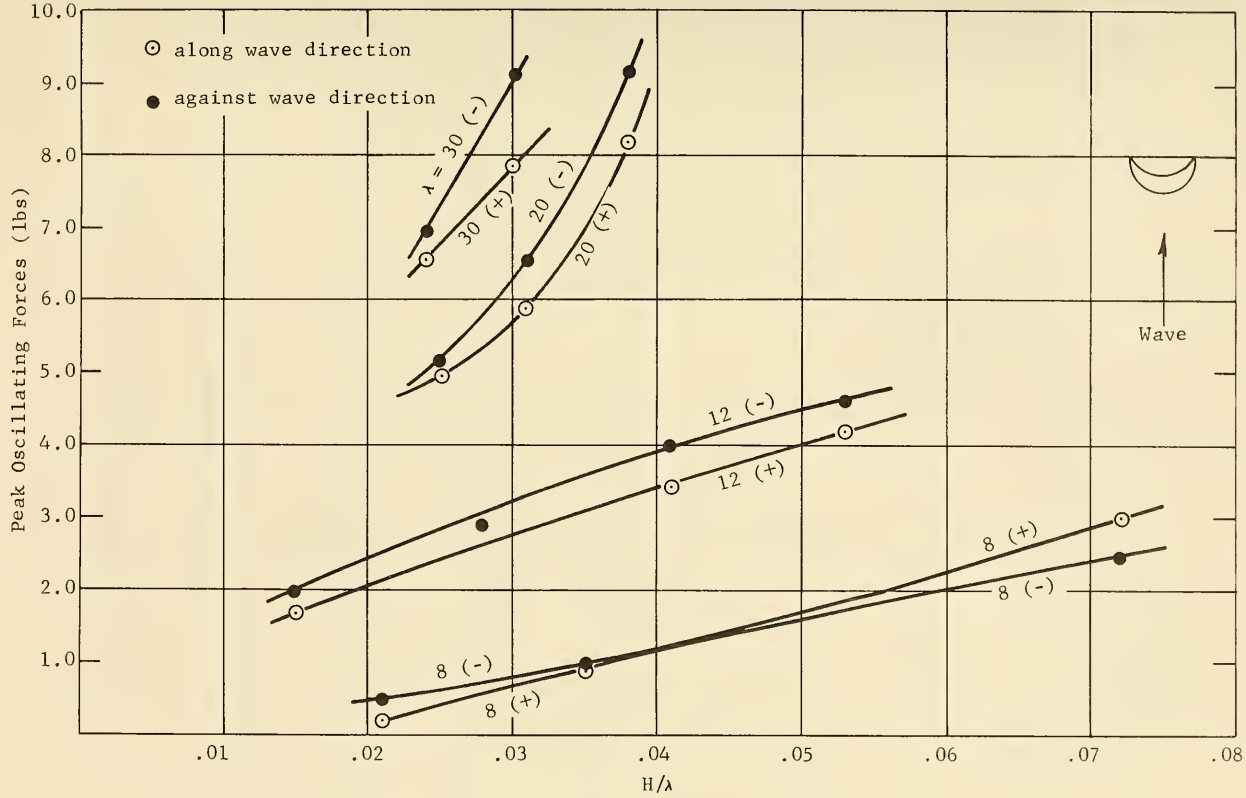

Figure 19. Wave forces on crescent shaped model - 300 series

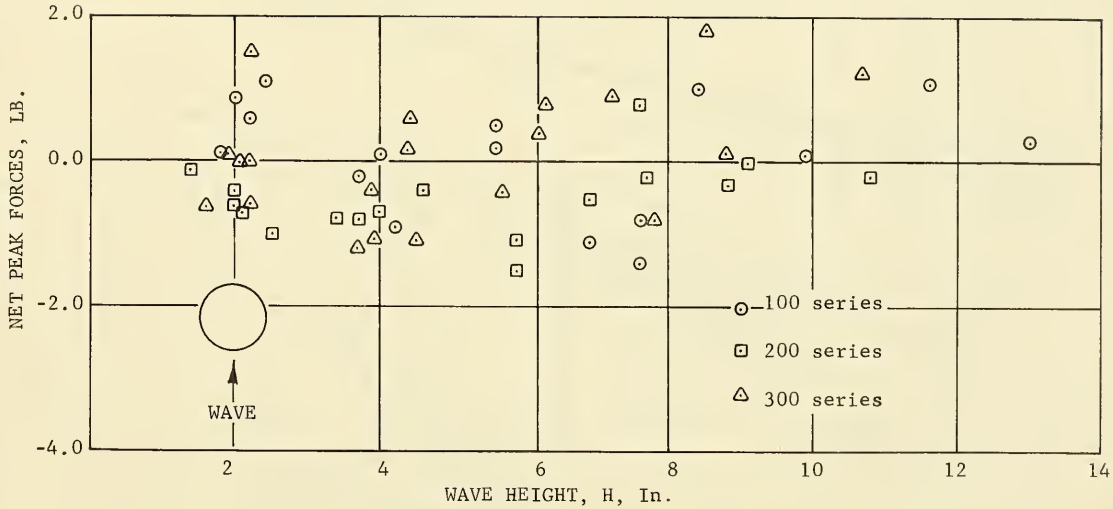

Figure 20. Net peak forces on circular model.

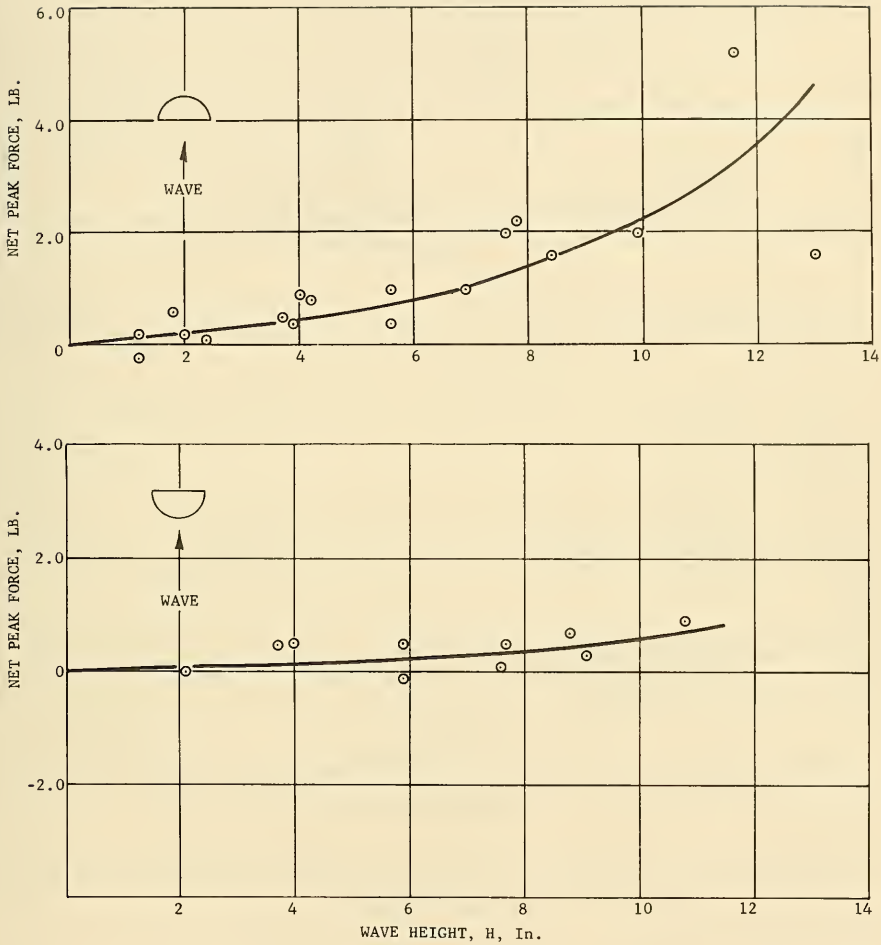

Figure 21. Net peak forces on semi-circular model.

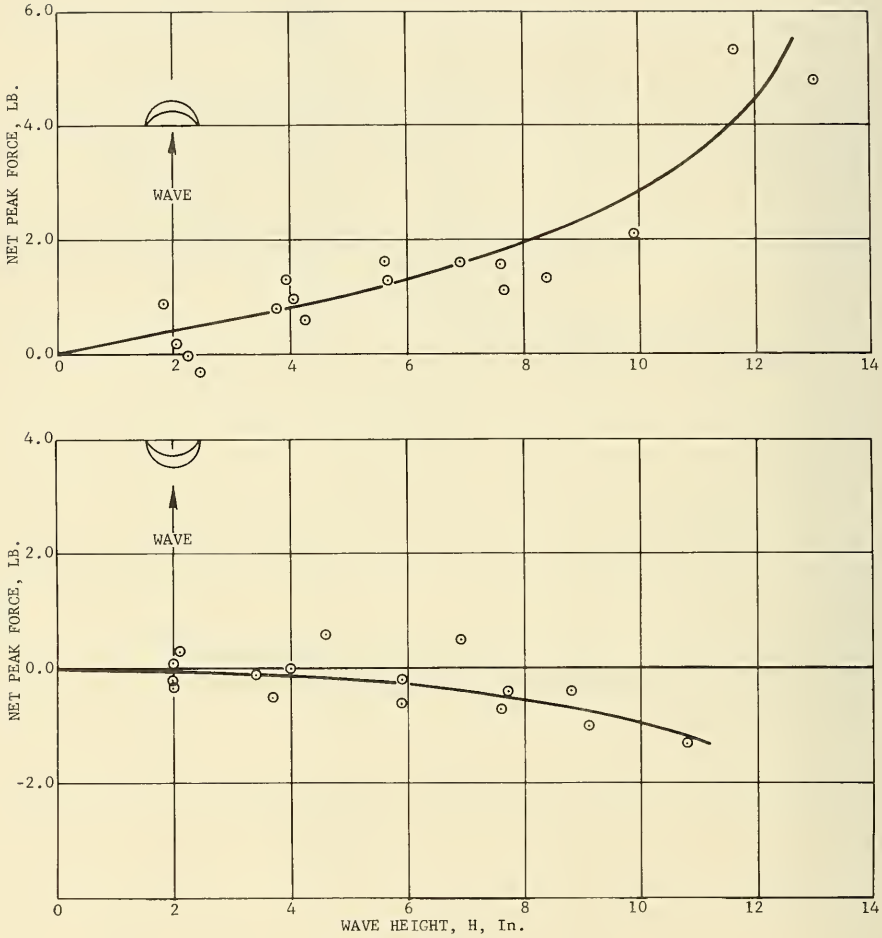

Figure 22. Net peak forces on crescent shaped model.

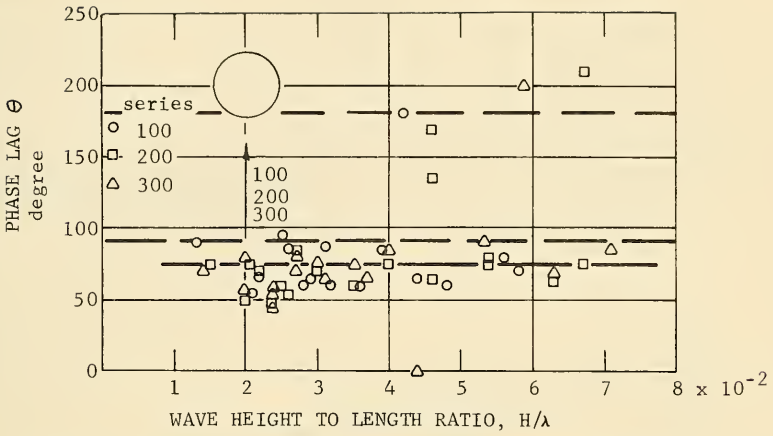

Figure 23. Phase lag of force data - Circular model.

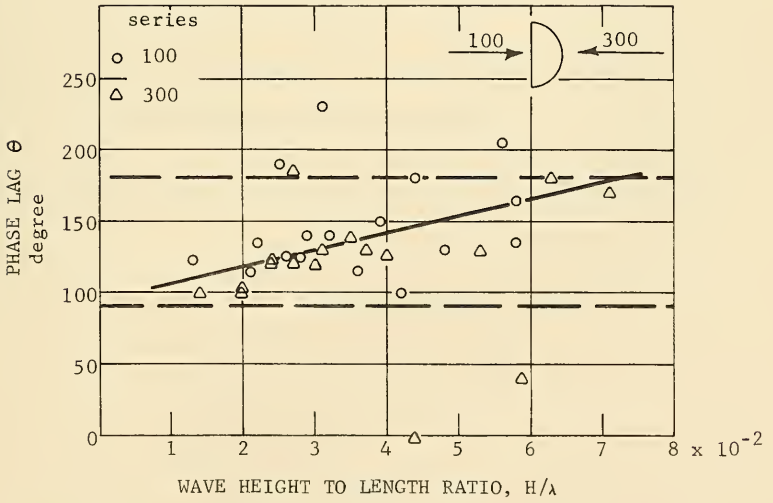

Figure 24. Phase lag of force data - Semi-circular model.

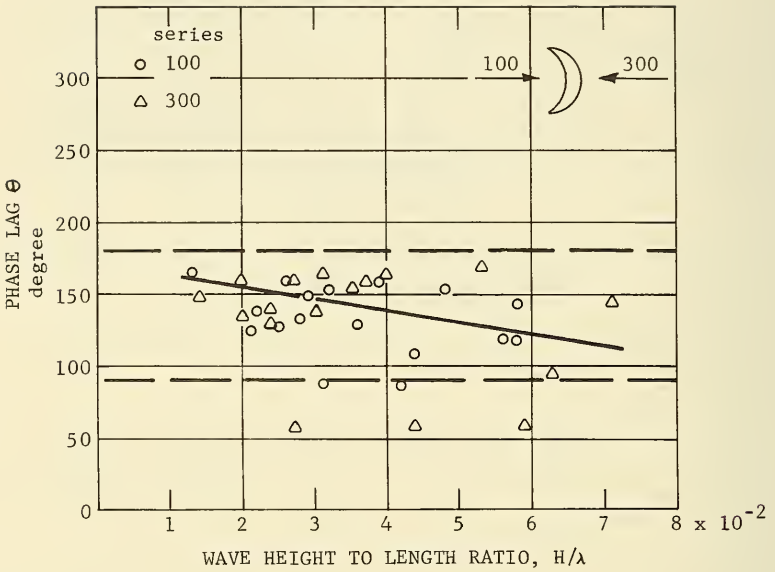

Figure 25. Phase lag of force data - crescent shaped model

REFERENCES

1. Weidlinger, Paul, Floating Airport, Ocean Industry, May 1970.

2. Rouse, H., Elementary Mechanics of Fluids, John Wiley & Sons, New York, 1946.

3. Nath, J. H. and D. R. F. Harleman, Response of Vertical Cylinder to Random Waves, Preprint, ASCE, Water Resource Engineering Meeting, New Orleans, La., February 1969.

NOMENCLATURE

A	cross-sectional area of object, ft^2
a	water particle acceleration, ft/sec^2
C_D	drag coefficient
C_{Df}	drag coefficient at wave side of model
C_{Dr}	drag coefficient at real side of model
C_I	inertia coefficient
D	diameter of pile, ft
F	total peak wave drag force on object, lb
F_f	total peak positive wave drag, lb
F_r	total peak negative wave drag, lb
f	wave frequency, Hz
f_n	model natural pitching frequency, Hz
H	wave height, in
L	submerged model length, ft
L_c	submerged model length at wave crest, ft
L_t	submerged model length at wave trough, ft
l	distance along the model, ft
P	local unit wave force, lb/ft
U	flow velocity in general, ft/sec
V	peak water particle velocity, ft/sec
$\bar{V}$	mean peak velocity, ft/sec
V_d	model drifting velocity, ft/sec
V_m	maximum peak water particle velocity in waves, ft/sec

v	local water particle velocity in waves, ft/sec
ρ	fluid mass density, slug/ft^3
μ	fluid kinematic viscosity, ft^2/sec
λ	wave length, ft
θ	phase lag, degree

PART II. THE FEASIBILITY OF HYDRODYNAMIC FORMS FOR STATION KEEPING OF A LARGE FLOATING PLATFORM

by

R. H. Fashbaugh, Ph.D.

INTRODUCTION

This section is a preliminary study to determine whether a hydrodynamic form for extracting energy from ocean waves is economical in providing partial station keeping forces for the buoyant column configuration of the Mobile Ocean Basing System (MOBS).

A brief explanation of the method in which the hydrodynamic forms extract energy from ocean waves is appropriate. A sketch of the subject hydrodynamic form is shown in Figure 1. The form cross section is crescent in shape which provides the characteristic that water flowing around the form in a direction that is into the concave side causes a drag force on the form that is higher than the drag force caused by water flowing at the same flowrate in the opposite direction. Associated with an ideal gravity wave on the surface of a deep body of water is a fluid motion in which the water particles move in circular closed paths. The diameter of these paths decays exponentially with increase distant from the water surface. The force on a circular cylinder, extending vertically into a body of water, that is caused by surface waves is an oscillating force. If the variation in water surface height is neglected the wave force on the cylinder will have peak values in the wave direction and opposite to the wave direction that are equal. When the circular cylinder is replaced by a hydrodynamic form which is oriented so that the concave side faces in the direction of wave travel the oscillating force due to the waves will have a larger peak value in the direction opposite to the direction of wave travel. The oscillating force on the form will therefore have an impulse over a wave period that is opposite to the direction of wave travel which will cause the form and any associated structure to move in that direction. The intent of this study is to estimate the magnitude of this force impulse and to assess its utilization for MOBS station keeping.

The problem of determining the magnitude of oscillating wave forces on the hydrodynamic form is by nature empirical. Testing is therefore required to determine empirical coefficients. Adequate coefficients were obtained from the NCEL tests described in Part I. In addition to the NCEL test results, the results of tests conducted at the University of California[1,2] on circular and flat piles were utilized. An analytical solution for the wave force in which these data are used is presented.

To supplement the analytical study a test was conducted in the NCEL wave tank in which the effect of the hydrodynamic forms on the drift velocity of a model floating platform, Figure 2, was determined. The results of this test are presented below.

ESTIMATION OF HYDRODYNAMIC FORM EFFECTIVENESS

Force Exerted by Surface Waves

The force exerted by surface waves on a cylindrical object which extends vertically into a body of water is made up of two components, a viscous drag force and a virtual mass force. The drag force component is proportional to the square of the horizontal component of the water velocity relative to the object and the virtual mass force component is proportional to the relative horizontal acceleration. From Morison[1] the force exerted on a differential section, dz, can be written as:

$$dF = \left[C_D \left(\frac{\rho D}{2} \right) u \, |u| + C_M \left(\frac{\rho \pi D^2}{4} \right) \frac{\partial u}{\partial t} \right] dz, \qquad (1)$$

where u is the horizontal component of velocity, D the cylinder diameter, ρ the water mass density, C_D the coefficient of drag, and C_M the coefficient of virtual mass. A theoretical expression is used for the velocity u in relation (1). Since there are several wave theories the choice of which one to use depends upon the degree to which it is desired to approximate non-linear ocean waves. For the purposes of this preliminary study the linear Airy wave theory for deep water will be adequate. Values for the empirical coefficients C_D and C_M are taken from References 1 and 2 to be consistent with the linear wave theory assumption.

The interest here is obtaining the wave force on a full scale hydrodynamic form by utilizing Equation (1). Because of the unusual shape of the cross section of this form values for the coefficient C_D and C_M are not available. There is available however from the NCEL model test data which can be used to compare the peak wave force for the crescent shape to the peak wave force for a circular section of equivalent diameter. Utilizing this, the wave force on a hydrodynamic form is considered related to the wave force on a circular cylinder by the relation:

$$\Delta F = K \, F_{cyl} \qquad (2)$$

where ΔF is the difference between positive and negative peak values of the oscillating force on the hydrodynamic form and F_{cyl} is the peak value of force on a circular cylinder subjected to the same wave train.

Values for the coefficient K determined from the NCEL test data are shown in Table 1.* Since there is not a sufficient amount of data to determine how K varies with the wave parameters the average value of 0.17 is used.

Table 1. Values of coefficient K - NCEL data.

L(ft)	H(ft)	H/L	ΔF(lbs)	F_{cyl}(lbs)	K
30	0.90	0.030	1.3	5.5	0.24
20	0.76	0.038	1.0	6.1	0.16
20	0.63	0.032	0.7	5.2	0.14
12	0.49	0.041	0.6	4.7	0.13

Average K = 0.17

H = Wave Height
L = Wave Length

Experimental data for wave forces on flat plate and cylindrical piles reported in reference 2 can be correlated with the data in Table 1 with fairly good agreement. The wave force in the direction of the concave side of the hydrodynamic form can be approximated by the wave force on a flat plate of the same length and width. Similarly, the wave force in the direction of the convex side of the form can be approximated by the force on a circular cylinder. With these assumptions, values for the coefficient K obtained from reference 2 are shown in Table 2. Breaking wave data which is given in the reference was omitted since the wave steepness ratios for the NCEL data were considerably below breaking wave values. The reference 2 data correlates well with the NCEL data.

Table 2. Values of coefficient K - Morison data (ref. 2).

L(ft)	H(ft)	H/L	K
7.54	0.681	0.0803	0.280
3.87	0.342	0.0884	0.170

*The data of Table 1 is obtained from Table 3 of Part I. Since ΔF involves differences of measured forces, small data values are not included to improve accuracy. The values of F_{cyl} are the averages of the data from the three series of tests.

The expression for the force F_{cyl} of Equation (2) is obtained by integration of Equation (1) over the submerged length of the form. Following reference (1), with coordinates as shown in Figure 3, leads to the expression:

$$F_{cyl} = \frac{\rho D H^2 g}{16}\left[-C_M\left(\frac{2\pi D}{H}\right)\left(1 - e^{-\frac{2\pi d}{L}}\right)\sin\theta_m + C_D\left(1 - e^{-\frac{4\pi d}{L}}\right)\cos^2\theta_m\right] \quad (3)$$

where

$$\theta_m = \frac{2\pi t_m}{T} = \sin^{-1}\left[-\frac{C_M}{C_D}\left(\frac{\pi D}{H}\right)\left(\frac{1 - e^{-\frac{2\pi d}{L}}}{1 - e^{-\frac{4\pi d}{L}}}\right)\right] \quad (4)$$

and H = Wave height

L = Wave length

T = Wave period

d = Mean wetted length of form

g = acceleration due to gravity

t_m = Time the maximum force leads the wave crest.

Consistent with the assumption of the Airy wave theory the expression for the velocity that was used in obtaining expression (3) is:[3]

$$u = \left(\frac{\pi H}{T}\right) e^{\frac{2\pi z}{L}} \cos\left(\frac{2\pi t}{T}\right) \quad (5)$$

The negative sign appears in expression (4) for θ_m, the angle between the maximum force and the wave crest, because the force always leads the wave and θ_m will therefore be in the fourth quadrant.

Momentum Change Caused by Net Force

In evaluating the effect of the wave force on the hydrodynamic form it is necessary to consider the momentum change due to this force in a wave period. Accordingly:

$$\Delta(Mv) = \frac{T}{2\pi}\int_0^{2\pi} F(\theta)\, d\,\theta, \quad (6)$$

where $\Delta(Mv)$ is the momentum change, $F(\theta)$ is the wave force, and $\theta = 2\pi t/T$ with t the time. When the virtual mass force component exceeds the viscous drag force component by at least 2.5 the viscous component can be neglected[4] and relation (6) can be approximated as (utilizing relation (2)):

$$\Delta(Mv) \approx \frac{T}{2\pi}\left[\int_0^{\pi} F_{cyl} \sin\theta \, d\theta + \int_{\pi}^{2\pi} (K + 1) F_{cyl} \sin\theta \, d\theta\right]$$

from which,

$$\frac{\Delta(Mv)}{T} \approx -\left[\frac{K}{\pi}\right] F_{cyl}, \qquad (7)$$

where F_{cyl} is given by Equation (3) and K = 0.17. From Equation (3) it can be seen that the ratio of the virtual mass force component to the viscous drag force component is proportional to D/H. For large diameters the viscous drag force component can be neglected up to fairly large wave heights. For the case of the example presented below the form diameter is 20 feet and, according to curves in reference (4), the neglection is accurate to wave heights up to 60 feet.

The momentum change per wave caused by the force on the hydrodynamic form of Figure 1 is given in Figure 4. The effect of a 5 foot and a 10 foot wave for various wave lengths is shown. These curves were obtained from relations (3) and (7) with $C_D = 1.6$ and $C_M = 1.5$.* In order to lend a physical meaning, the momentum change that is caused by a one knot and a one-half knot current flowing in the direction of wave travel (into the convex side of the form) is also shown. At intersection points between a wave force curve and a current curve the effect of the crescent form is to cause an impulse that is equal in magnitude to the impulse of the current drag force but opposite in direction; e.g., with a wave of 10 foot height and 500 foot length and a one knot current the net momentum change is zero and the net movement of the hydrodynamic form under these conditions would be zero. The steady current flow of one knot creates a drag force of 6480 lbs on the form which is equivalent to approximately 20 hp. Therefore, with the particular wave condition stated above, the hydrodynamic form extracts energy from the waves at the net rate of approximately 20 hp.** The sea state example taken is in the range of seas classed as state No. 5 (rough sea).

---

*Based on references (5) and (6), C_D and C_M are considered not to vary significantly with Reynolds number.

**Net energy rate refers to that energy available for net motion opposite to wave direction.

MOBS Example 1

In order to evaluate the hydrodynamic form effectiveness on a floating platform, a configuration similar to Figure 2 is assumed. The hypothetical platform is 300 feet by 300 feet with 36 buoyant columns of 20 foot diameter and 100 foot submerged length and with 12 hydrodynamic forms. Assuming a 2 knot current and a 40 knot wind environment (references 7 and 8) the required propulsion system output is estimated as 17,100 hp (refer to Appendix A). For a sea state condition of 5 the hydrodynamic form net rate of energy extraction is approximately 240 hp. The effect of the hydrodynamic forms for this configuration and environment is 1.4% of the estimated required propulsion system output.

MOBS Example 2

A second case is considered in which all of the 36 buoyant columns of the configuration assumed in Example 1 have the hydrodynamic shape. The same environment of a 2 knot current and a 40 knot wind is assumed. The estimated propulsion system requirement is the same value of 17,100 hp. For a sea state condition of 5 the hydrodynamic form rate of energy extraction is approximately 960 hp which is 5.6% of the estimate required propulsion system output.

A parametric study is beyond the scope of this preliminary study. However, the results of the above examples strongly indicate that the effectiveness of the hydrodynamic form is not too significant.

MODEL TEST

Introduction

To supplement the analytical study and to improve insight into the problem a floating platform model test was conducted in the NCEL wave tank. The model consisted of an aluminum sheet platform with thirty wooden buoyant columns of one inch diameter and fourteen inch length as shown in Figure 2. Attached as shown in the figure were eight wooden hydrodynamic forms of twelve inch length and one and one half inch equivalent diameter.

Test Procedure

The average drift velocity of the model was measured over a drifting length of five feet for wave steepness ratios up to 0.130 (H/T^2 to 8.0). Drift velocities were measured for two orientations of the model: the normal orientation in which the concave side of the hydrodynamic form is facing in the direction of wave travel and the orientation opposite to this in which the concave side faces opposite to the direction of wave travel. The effect of the hydrodynamic forms in the normal orientation

is to reduce the model drift velocity in the direction of wave travel and, conversely, the effect is to increase the drift velocity when the forms are in the opposite direction.

Mechanics of Drift

To aid in the interpretation of the test results the mechanics of the wave forces which cause the model to drift will be discussed. First, it is important to note that an object floating on the surface of the water in the wave tank did not drift for the wave conditions used in the test. The drift of the MOBS model is caused by unequal wave forces on the buoyant columns. This inequality in forces is due to the wave acting over a longer portion of the buoyant column when a wave crest passes than when a wave trough passes. There is therefore a net force impulse in the direction of wave travel which causes the model to drift. Pitching and heaving motions of the model will considerably effect the length of the bouyant column over which the wave acts. The drift velocity is therefore influenced by the motion of the model. This fact makes the establishment of a meaningful baseline using a model without hydrodynamic forms very difficult. For this reason the effect of the forms was established by comparing the drift velocity with the forms in the normal orientation to the drift velocity with the forms in the opposite orientation.

Test Results

The results of the test are presented in Figure 4. The model drift velocity is shown in the lower curve for the normal hydrodynamic form orientation and in the upper curve for the opposite orientation. The dotted line represents the mean between the upper and lower curves. The effect of the hydrodynamic form on the drift velocity is estimated as the difference between the lower curve and the mean curve. This comparison is considered the most accurate when the model was stable which was outside of the region represented by values of H/T^2 from 0.6 to 4.8. For the very long wave lengths the model was stable and drifted opposite to the direction of wave travel with very little relative motion between the model and the surface of the water. This case corresponds to the extreme left end of the lower curve. For the short wave lengths corresponding to values of H/T^2 greater than 4.8 the model was very stable with very little pitch or heave. There is no apparent explanation for the peaking of the upper curve in the range of H/T^2 of 2.0 except possibly the fact that the model was pitching considerably. The region does not, however, correspond to the natural pitch or heave periods of the model as one might expect.

Summary of Findings

A summary of findings based on test observations and data is given below:

1. For wave lengths long compared to the model length the hydrodynamic forms extracted sufficient net energy from the waves to cause model drift opposite to the direction of wave travel.

2. For short wave lengths of the order of magnitude of model length the effect of the hydrodynamic forms was to reduce the drift velocity in the direction of wave travel approximately 10%. This suggests that the net force impulse due to the shape of the hydrodynamic forms is small compared to the net force impulse due to the water surface level variations.

3. The model drift was affected considerably by the motion of the model with respect to the water surface.

4. The mechanics of drift of floating platforms suppored by vertical buoyant columns differs considerably from the mechanics of drift of platforms floating on the surface of the water.

CONCLUSIONS

Since the rate of energy extraction from waves by hydrodynamic forms was estimated for sea state No. 5 to be only approximately 6% of the energy required to maintain station, the concept does not seem applicable to large floating ocean platforms.

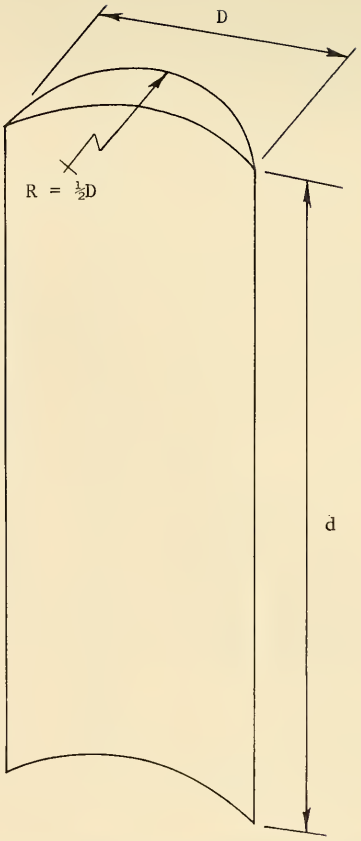

Figure 1. Sketch of Hydrodynamic Form

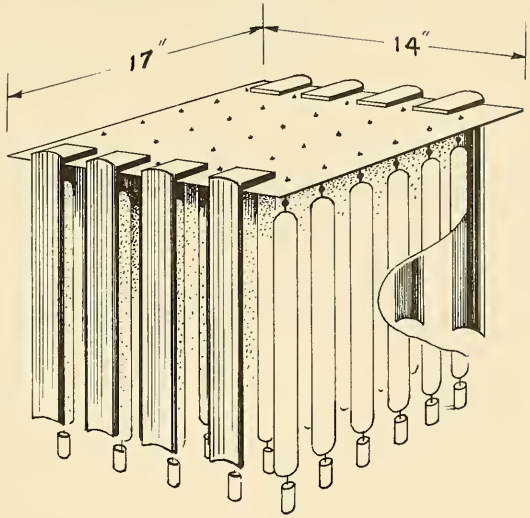

Figure 2. Model for Hydrodynamic Form Test

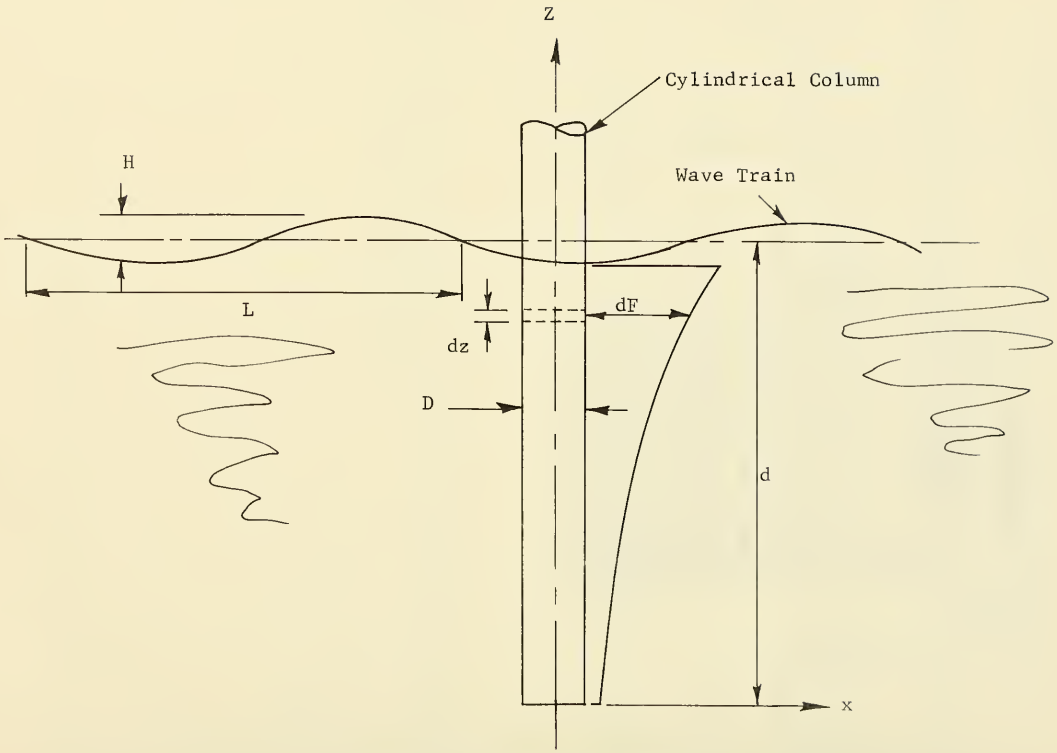

Figure 3. Definition Sketch

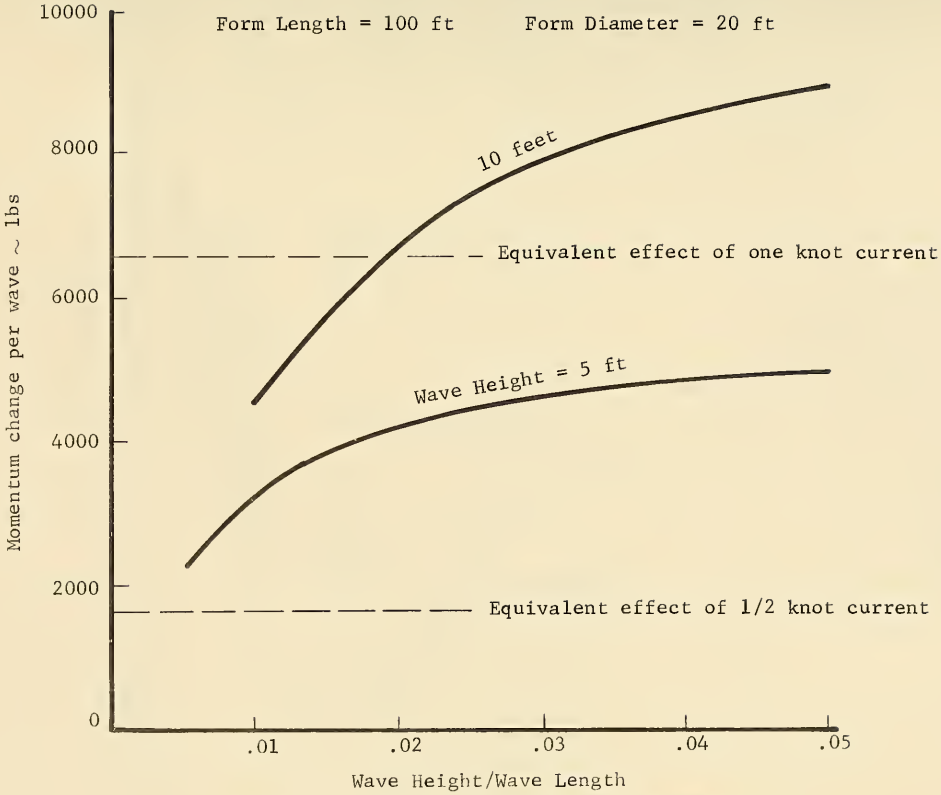

Figure 4. Effect of Hydrodynamic Form Net Force

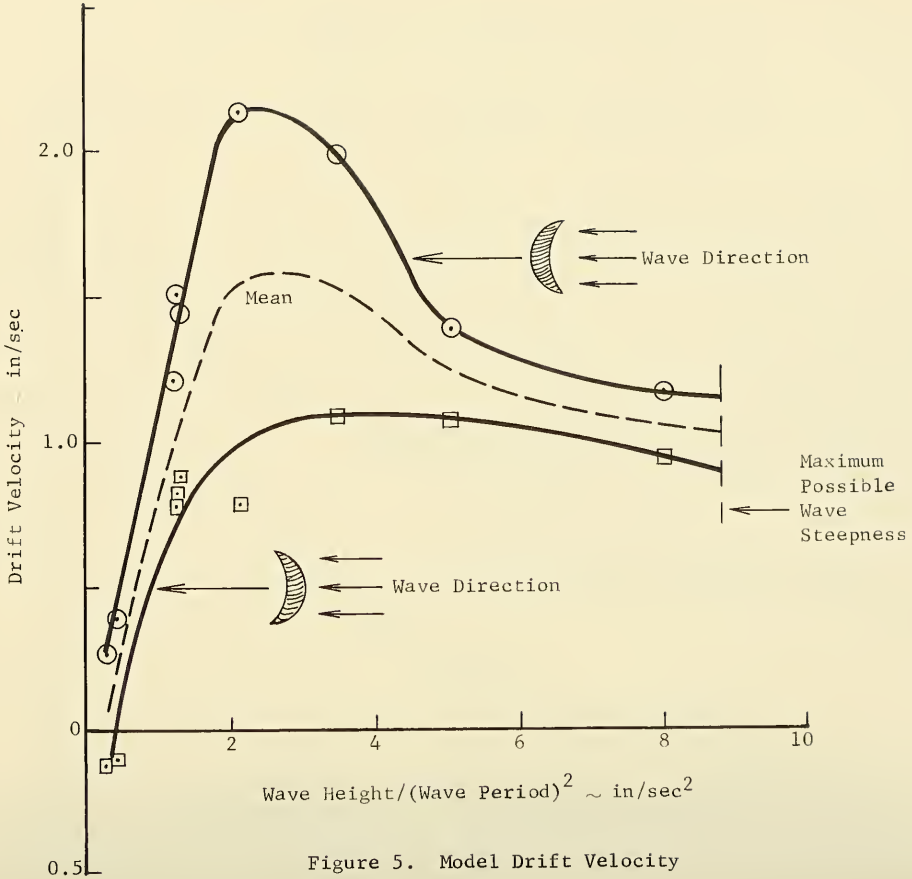

Figure 5. Model Drift Velocity

Appendix A

ESTIMATION OF FLOATING PLATFORM STATION KEEPING POWER REQUIREMENTS

Consider a platform of the following configuration:

1. Dimensions; 300 ft by 300 ft.

2. 36 bouyant columns; 20 foot diameter and 100 foot wetted length.

3. 12 hydrodynamic forms; 20 foot diameter and 100 foot wetted length.

4. 20 foot spacing from platform to water.

5. Platform structure height of 20 feet.

The environmental conditions are taken to be an ocean current of 2 knots and a wind velocity of 40 knots.

The power requirements to maintain station are estimated as:

$$P = \frac{F_c\ V_c}{550} + \frac{F_w\ V_w}{550} = 7700 + 9400 = 17{,}100 \text{ hp}$$

where F_c = current drag force $\approx 1/2\ \rho\ C_D\ AV^2 \times 48$

$= 1/2 \times 1.99 \times 1.2 \times 20 \times 100 \times (1.69 \times 2)^2 \times 48$

$= 1.27 \times 10^6$

$$\frac{F_c\ V_c}{550} = \frac{1.27 \times 10^6 \times 1.69 \times 2}{550} = 7700 \text{ hp.}$$

Similarly, F_w = wind drag, and

$$\frac{F_w\ V_w}{550} \approx 1/2 \times 0.002378 \times 1.2 \times (300 \times 40) \times (1.69 \times 40)^3 \times \frac{1}{550} = 9400 \text{ hp.}$$

Appendix B

ESTIMATE OF COST OF A HYDRODYNAMIC FORM INSTALLATION

In the following is an approximation of the cost of a 20 foot diameter - 100 foot long hydrodynamic form fabricated of steel including the associated structure and equipment.

1. Cost of form construction assuming a shell thickness of 3/8".

(a) Material Cost

$$\text{Material volume} = \pi \times 20 \times \frac{.375}{12} \times 100$$

$$= 197 \text{ ft}^3$$

Material weight = 197 x 490 = 96,500 lbs

Cost of form material at $.30 per lb = $29,000.

Assuming the weight of the support structure and ribs as 3/4 of the form weight; total cost of material for support structure and ribs = 3/4 x 29,000 = $22,000; total cost of material = 29,000 x 22,000

= $51,000

(b) Fabrication Cost

Cost of fabrication at $.60 per lb = .60 x 96,500 x 1.75

= $100,000.

2. Cost of mechanical equipment to rotate form.

The main energy dissipation associated with rotation of the form is that due to water drag resistance.

$$\text{Water resistance torque} \approx 1/2 \, C_D \, A \, \rho \, V^2 \times \frac{D}{4}$$

where, $V \approx 2\pi f \times \frac{D}{4} = \frac{10\pi}{60} \times 5 = 2.62$ ft/sec, for f = 5 rpm.

$A = 100 \times 20 = 2{,}000 \text{ ft}^2$

$\rho = 1.94$ slugs/ft^3

$C_D = 1.2$

Torque $\approx 1/2 \times 1.2 \times 2000 \times 1.94 \times (2.62)^2 \times 5$

$= 80{,}000$ ft lb

Power Required $= \frac{2\pi f \times T}{550} = \frac{10\pi}{60} \times \frac{80{,}000}{550} = 76$ hp.

Allowing for friction losses in the gear box and support bearings the hp requirements are estimated to be about 2 x 76 = 152 hp. At $50. per hp the cost of mechanical equipment = 152 x 50 = $7,600.

3. The total cost from the above is summarized in the following table.

Material, including support structure	$ 51,000
Fabrication	100,000
Associated mechanical equipment	7,600
Total estimated cost	$158,600

REFERENCES

1. "The Force Exerted by Surface Waves on Piles," by J. R. Morison, et al, J. of Pet. Tech., Vol. 2, No. 5, May 1950.

2. "Experimental Studies of Forces on Piles," by J. R. Morison, et al, Proc., of 4th Conf. on Coast. Engr., Chicago, October 1953.

3. "Wind Waves," by Blair Kinsman, Prentice-Hall, Inc., 1965.

4. "Response of Vertical Cylinders to Random Waves," by J. H. Nath and D. R. F. Harleman, J. of Waterways and Harbors Div., Proc. A.S.C.E., May 1970.

5. "Analysis of Wave Force Data," by D. J. Evans, Offshort Tech. Conf., Dallas, 1969.

6. "Wave Forces: Data Analysis and Engineering Calculation Method," P. M. Aagaard, Offshore Tech. Conf., Dallas, 1969.

7. "Floating Ocean Research & Development Station," Final Report, J. McDermott & Co., Inc., April 1966.

8. "Environmental Analysis Relative to Portable Port Operations," Ocean Sciences and Engineering, Inc., November 1969, Report prepared for NCEL.

DISTRIBUTION LIST

SNDL Code	No. of Activities	Total Copies	
-	1	12	Defense Documentation Center
FKAIC	1	10	Naval Facilities Engineering Command
FKNI	6	6	NAVFAC Engineering Field Divisions
FKN5	9	9	Public Works Centers
FA25	1	1	Public Works Centers
-	9	9	RDT&E Liaison Officers at NAVFAC Engineering Field Divisions and Construction Battalion Centers
-	304	304	NCEL Special Distribution List No. 9 for persons and activities interested in reports on Deep Ocean Studies

Unclassified
Security Classification

DOCUMENT CONTROL DATA - R & D

(Security classification of title, body of abstract and indexing annotation must be entered when the overall report is classified)

1. ORIGINATING ACTIVITY (Corporate author)

Naval Civil Engineering Laboratory
Port Hueneme, California 93041

2a. REPORT SECURITY CLASSIFICATION
Unclassified

2b. GROUP

3. REPORT TITLE

Wave Energy Extraction By Crescent Shaped Columns For Station Keeping Of Floating Ocean Platforms - Hydraulic Model And Feasibility Study

4. DESCRIPTIVE NOTES (Type of report and inclusive dates)

5. AUTHOR(S) (First name, middle initial, last name)

C. L. Liu
R. H. Fashbaugh

6. REPORT DATE	7a. TOTAL NO. OF PAGES	7b. NO. OF REFS
March 1971	59	11

8a. CONTRACT OR GRANT NO.	9a. ORIGINATOR'S REPORT NUMBER(S)
b. PROJECT NO. ZF 38.512.001.017 03-001	TN-1156
c.	9b. OTHER REPORT NO(S) (Any other numbers that may be assigned this report)
d.	

10. DISTRIBUTION STATEMENT

Approved for public release; distribution unlimited.

11. SUPPLEMENTARY NOTES	12. SPONSORING MILITARY ACTIVITY
	Office of Naval Research and Director of Navy Laboratories

13. ABSTRACT

Fixed or floating column-supported platforms in the ocean experience direct and reverse wave drag caused by the oscillating water particle velocity. The drag coefficient for the direct flow can be different from that for the reverse flow if the cross-sectional area of the supporting column is not symmetric about the column axis. Therefore, a net wave drag force theoretically can be produced. The purpose of this study was to determine whether this concept can be utilized to reduce the power requirements for positioning large floating platforms such as the proposed Mobile Ocean Basing System (MOBS).

Two support column cross sections were chosen for evaluation; a semi-circle and a crescent shape which is formed by two intersecting circles (the larger circle having a radius 1-1/2 times that of the smaller circle). A circular cross section was included to provide a reference. Free drift velocity tests of three small scale tri-column platforms with the three different cross sections were made in a small wave tank as a preliminary experiment. Based on the results of this drift experiment wave drag measurements were made with larger

Continued

14 KEY WORDS	LINK A		LINK B		LINK C	
	ROLE	WT	ROLE	WT	ROLE	WT
Floating platforms						
Platforms						
Ocean currents						
Hydrodynamics						
Water waves						
Wave drag						
Hydrodynamic configurations						
Loads (forces)						
Station keeping						
Oceans						

single column models of 4 inch diameter and 8 foot length in a large wave tank. Free drift velocity tests were also conducted with a 14 inch by 17 inch rectangular model floating platform with 36 supporting columns to aid in evaluating the concept for MOBS use.

The results of the tests show that there is a net wave force opposite to the direction of wave travel on the column with the crescent cross section. However, an analytical study based on the test data shows the rate of energy extraction from waves by crescent shaped columns for sea state 5 to be about 6% of the energy required for station keeping of a large floating platform. Hence, the concept does not seem applicable to large floating ocean platforms.